

The Design of a Small and Inexpensive Abrasive Waterjet Cutter

by

FELIPE VARELA

B.S., Mechanical Engineering
Georgia Institute of Technology, 1997

SUBMITTED TO THE DEPARTMENT OF MECHANICAL ENGINEERING
IN PARTIAL FULFILLMENT OF THE DEGREE OF

MASTER OF SCIENCE IN MECHANICAL ENGINEERING

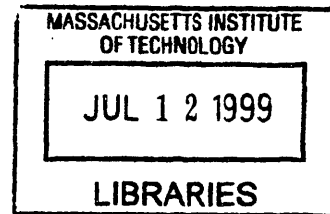
at the

MASSACHUSETTS INSTITUTE OF TECHNOLOGY

June 1999

© 1999 Massachusetts Institute of Technology
All rights reserved

ARCHIVES



Signature of Author
Department of Mechanical Engineering
May 21, 1999

Certified by
Alexander Slocum
Professor of Mechanical Engineering
Thesis Advisor

Accepted by
Ain A. Sonin
Chairman, Department Committee on Graduate Students

The Design of a Small and Inexpensive Abrasive Waterjet Cutter

by

FELIPE VARELA

Submitted to the Department of Mechanical Engineering
on May 6, 1999 in Partial Fulfillment of the
Requirements for the Degree of Master of Science
in Mechanical Engineering
at the Massachusetts Institute of Technology

ABSTRACT

The design of a small and inexpensive abrasive waterjet cutter was carried out and documented from the specification of functional requirements through to final design and solid modeling. Starting from the identification of the functional requirements for the machine, several concepts were generated, compared and selected for further analysis. The selected concepts were then further analyzed and compared using error budgeting and cost considerations. One concept, featuring an X-Y system of motion was then selected and developed.

The small working area of the machine, 13 inches by 26 inches, allowed for the X-Y concept to be developed into a design that used off-the-shelf linear guide rails as the structure of the machine. A bench-level prototype of this structure was built and tested to prove the concept and optimize the design. Once structural testing and stiffening/damping technique testing was completed, the entire machine was designed and solid modeled on Pro/ENGINEER.

The bare-rails structure resulted in a design that requires fewer precision-machined parts and fewer parts overall, resulting in a design that is inexpensive to manufacture and assemble.

Thesis Supervisor: Prof. Alexander Slocum

Title: Professor Of Mechanical Engineering

ACKNOWLEDGMENTS

Thanks first and foremost to God for giving me the talents and abilities to get this far.

Thanks to Alex Slocum for being the best thesis advisor I can imagine. He took me on board and worked with me to find an awesome thesis project. His guidance and seemingly infinite wisdom and experience provided a great working and learning experience.

Thanks to all the grad students in Alex's lab for making it a great place to work, I can't imagine working with a nicer bunch of people. The PhD candidates were a generous source of information, their knowledge and experience were invaluable in completing this thesis. Thanks to Marty Culpepper for his mentoring during the early stages of my project. His input and assistance made for an smooth start, as smooth as one can be. Thanks to Nathan Kane for his endless patience. Little did he know when he switched offices and ended up occupying the desk next to mine that he would become the target for my endless questions. Ebbe Bamberg's knowledge and experience with machine tool design and FEA, and his willingness to answer my questions regarding them, played an important part in the completion of this thesis. Thanks to Don O'Sullivan for his willingness to always provide any assistance or answer questions, and also for his invaluable thesis template. Thanks to Joachim Sihler for his help in machining some of the components for my bench-level prototype.

Thanks to Samir Nayfeh and his students, Kripa Varanasi and Andreas Athanassopoulos, for all their help with the modal testing and vibration analysis conducted on the bench-level prototype.

Thanks to Gerry Wentworth and Mark Belanger in the the LMP machine shop for their always-present willingness to help and their endless patience, and for teaching me so much about machining.

Thanks to Jason Jarboe for his help with the bench-level prototype, for helping me on numerous occasions to dismantle and reconfigure the prototype for the variety of tests that were conducted. Jason's input on the design of the machine and its components was very helpful, as well as his assistance in estimating the cost of parts and manufacturing. Many thanks also in advance for his work on the construction of my design.

Thanks to Scott Spangler at Star Linear for his generous donations which made it possible to construct and test the bench-level prototype. Thanks to the people at OMAX for their input and guidance.

I also wish to thank my mom and the rest of my family for their love and support, and I would like to dedicate this thesis to the loving memory of my dad, espero que estes orgulloso.

Abstract	3
Acknowledgments	5
Chapter 1. Introduction	15
1.1 Background	15
1.2 Concept Generation	16
1.2.1 Concept One	17
1.2.2 Concept Two	18
1.2.3 Concept Three	19
1.2.4 Concept Four	20
1.2.5 Concept Five	21
1.2.6 Concept Six	21
1.2.7 Concept Seven	23
1.3 First Pass Comparison and Elimination	24
Chapter 2. Concept Selection	25
2.1 Error Budget	25
2.1.1 The Homogeneous Transformation Matrix Model of the Machine	26
2.1.2 X-Y Concept	28
2.1.3 R- θ Concept	33
2.1.4 θ - θ Concept	35
2.2 Concept Comparison	37
2.3 Summary and Conclusion	39
Chapter 3. X-Y Concept Preliminary Design	41
3.1 Optimal Structural Cross-Section	41
3.1.1 Maximization of Torsional Stiffness	41
3.1.2 Finite Element Analysis	43
3.2 Conception of Rails-Only Structure	47
3.2.1 Analysis of Bare-Rail Design	47
3.2.2 Second Pass FEA Analysis	51
Chapter 4. Structural Testing	55
4.1 Single Long Ball Bearing Truck	57
4.1.1 Straightness	57
4.1.2 Yaw	58
4.1.3 Static Stiffness	60

4.1.4	Dynamic Stiffness	61
4.2	Single Long Cylindrical Roller Bearing Truck	64
4.2.1	Straightness	64
4.2.2	Yaw	65
4.2.3	Static Stiffness	66
4.2.4	Dynamic Stiffness	67
4.3	Two Standard Ball Bearing Trucks	69
4.3.1	Static Stiffness	69
4.3.2	Dynamic Stiffness	70
4.4	Stiffener and Damper Testing	71
4.4.1	Stiffeners	71
4.4.2	Damper	73
4.4.3	Longer Y-axis Rail	74
4.5	Summary and Conclusion	75
Chapter 5.	Final Design and Solid Modeling	77
5.1	Ball Rail and Ballscrew System	77
5.2	Bearing Blocks	79
5.2.1	X-Axis Motor Mount Bearing Block	80
5.2.2	X-Axis Encoder Mount Bearing Block	81
5.2.3	Y-Axis Motor Mount Bearing Block	83
5.2.4	Y-Axis Encoder Mount Bearing Block	83
5.3	Carriages and Ball Nut Mounting	84
5.4	Motors and Encoders	85
5.5	Sealing	86
5.6	Tank	89
5.7	Bill of Materials and Cost	91
5.8	Conclusion	92
5.9	Future Work	93
References		95
Appendix A.	Engineering Drawings	97

Figure 1.1	Sketch of Concept One	17
Figure 1.2	Sketch of Concept Two	19
Figure 1.3	Sketch of Concept Three	20
Figure 1.4	Sketch of Concept Four	21
Figure 1.5	Sketch of Concept Five	22
Figure 1.6	Sketch of Concept Six	22
Figure 1.7	Sketch of Concept Seven	23
Figure 2.1	Schematic of the X-Y concept	28
Figure 2.2	Kinematic Model for X-Y Concept	29
Figure 2.3	Example Member Shape and Dimension Input Window	32
Figure 2.4	Example Error Calculation Segment of Spreadsheet	32
Figure 2.5	Example Error at Tip Display Segment of Spreadsheet	33
Figure 2.6	Schematic of the R- θ Concept	34
Figure 2.7	Schematic of the θ - θ Concept	35
Figure 2.8	Kinematic Model for θ - θ concept	36
Figure 3.1	Bellows Diameter Spreadsheet Comparison of Results	43
Figure 3.2	Solid Model of Rectangular X-axis	44
Figure 3.3	Solid Model of C-channel X-axis	45
Figure 3.4	Solid Model of Rectangular X-axis Oriented Vertically	46
Figure 3.5	Solid Model of Size 55 Bare Rail as X-Axis	48
Figure 3.6	FEA Results for Bare Rail as X-Axis	48
Figure 3.7	Solid Model of Size 55 Rail X-Axis and Size 35 Rail Y-Axis	49
Figure 3.8	FEA Results for Size 55 Rail X-Axis and Size 35 Rail Y-Axis	49
Figure 3.9	FEA Results of Size 55 Rails for Both Axes	50
Figure 3.10	Solid Model of Bench-Level Prototype	51
Figure 3.11	FEA Results of the Bench-Level Prototype with One Ball Truck	53
Figure 4.1	Pro/ENGINEER Model of Experimental Setup	56
Figure 4.2	The Bench Level Prototype System	56
Figure 4.3	Rail Straightness Plot	58
Figure 4.4	Schematic of Yaw Test Setup	59
Figure 4.5	Yaw Error, Long Ball Bearing Truck	59

Figure 4.6	Static Vertical Stiffness at End of Cantilever	60
Figure 4.7	Frequency Response, Vertical, No Weight	62
Figure 4.8	Frequency Response, Vertical, With Weight	63
Figure 4.9	Frequency Response, Lateral, No Weight	63
Figure 4.10	Frequency Response, Lateral, With Weight	64
Figure 4.11	Rail Straightness, Cylindrical Roller Bearings	65
Figure 4.12	Yaw Error, Long Cylindrical Roller Bearing Truck	66
Figure 4.13	Static Stiffness, Cylindrical Roller Bearings	67
Figure 4.14	Frequency Response, Vertical, Weight	68
Figure 4.15	Frequency Response, Lateral, Weight	68
Figure 4.16	Static Stiffness, 2 Standard Ball Bearing Trucks	69
Figure 4.17	Frequency Response, 2 Trucks, Vertical, Weight	70
Figure 4.18	Frequency Response, 2 Trucks, Lateral, Weight	71
Figure 4.19	Frequency Response with Solid Stiffener Along X-axis	72
Figure 4.20	Frequency Response with Solid Stiffener and Damping Layer	73
Figure 4.21	Frequency Response for 31" Rail with 2 Trucks and Solid Stiffener	74
Figure 5.1	Rail Assembly	78
Figure 5.2	Assembly Showing Ballscrew Locations	78
Figure 5.3	FEA Results From Bearing Block Analysis	80
Figure 5.4	X-Axis Motor Mount Bearing Block	81
Figure 5.5	Exploded View of X-axis Motor Mount Bearing Block Assembly	82
Figure 5.6	Y-Axis Encoder Mount Bearing Block	82
Figure 5.7	Y-Axis Motor Mount Bearing Block	83
Figure 5.8	Y-Axis Encoder Mount Bearing Block	84
Figure 5.9	Exploded View of Y-Axis Encoder Mount Bearing Bock Assembly	84
Figure 5.10	Ballscrew Nut Mounting	85
Figure 5.11	Solid Model Showing Maximum and Minimum Bellows Lengths	87
Figure 5.12	Mountplate Showing Grooves for Internal Bellows Guide Rods	87
Figure 5.13	Assembly of the Small Waterjet Showing Bellows and Internal Guide Rods	88
Figure 5.14	Enclosures Sealing Components between Bellows	89
Figure 5.15	Polymer Concrete Tank	90

Figure 5.16 Solid Model of Finished Design 94

TABLE 1.1	First Pass Comparison of Concepts	24
TABLE 2.1	Summary Table of Error Budge and Concept Comparison	40
TABLE 3.1	Summary of FEA Modal Results, Rectangular vs. C-channel	45
TABLE 4.1	Summary of Frequency Response for all Configurations	75
TABLE 5.1	Bill of Materials and Cost of Machine	92

Chapter 1

INTRODUCTION

1.1 Background

An abrasive waterjet cutter is a machine that uses a fine stream of ultra-high pressure and fast-moving water mixed with abrasive to cut through most any type of materials. A specialized, ultra-high pressure pump creates a pressure of about 40,000 psi. The resulting jet of water is then mixed with a special sand-like abrasive and is then directed through a specialized nozzle at the workpiece to be machined. This type of machining system has many advantages. First, due to the low-force nature of the cutting process, there is no problem with fixturing the workpiece. Hence, setup time is minimal and more time can be spent on value-added machining of the parts. Second, since the cutting “tool” is a jet of water, many complex shapes can easily be cut where comparable shapes would be very expensive and complex by conventional machining methods.

This thesis develops a design for a small and inexpensive waterjet cutter. A machine that is targeted toward different markets than the full size abrasive waterjet cutters currently used in industry. It will be used as a supplement to, or an alternative for wire EDM (Electrical Discharge Machining), where complex-shaped machining of small parts takes place. In addition, this machine will be inexpensive enough so that it can be placed in hardware stores and small machine shops so that consumers can custom cut ceramic tiles, sheet metal, wood, etc., practically any type of material requiring custom cutting.

The machine to be defined had to follow some pre-defined functional requirements set by the customer. Some of these included:

- 26 in x 26 in machinable area
- Top speed 180 in/min
- Max acceleration .1 g's
- Resolution of .0005 in/step or finer
- Circularity of .003 in around a 12 in diameter circle running at max speed
- Cost of table, arm, and controls around \$10,000 or less

1.2 Concept Generation

To begin with, seven different general design concepts were developed and compared using simple physics calculations and a rough cost estimate, taking into account how many of the same elements each concept would require. Inherent to a waterjet cutter, each design incorporates a water tank as the base, the differences between the concepts are in the system of nozzle movement above the workspace.

In order to do a first pass comparison of the concepts, simple calculations are carried out to find the moment load on the bearings and the vertical deflection at the nozzle tip at its worst case position. The moment load of the bearings is relative to the cost of the bearings, since price increases with the amount of moment load they are made to support. The deflection will be indicative of the better designs as zero deflection is desired. Additionally, greater deflection means more material is required, resulting in more expense.

For simplicity in this concept generation stage, all structural members are assumed to be aluminum and to have a square cross-section with side lengths of six inches. Also, the weight of the nozzle and supporting components is assumed to be a 4.54 kg (10 pounds) point load at the end of the beam. In addition, a relative cost comparison is carried out by listing the number of similar components that each concept requires.

1.2.1 Concept One

Concept One uses an X-Y axis system suspended above the work space. The x-axis is aligned with the back of the machine and the entire y-axis travels back and forth on it. The y-axis is made up of a cantilever arm extending over the workspace on which the nozzle travels back and forth.

Figure 1.1 is a sketch of concept one. This design uses two linear motion guides and actu-

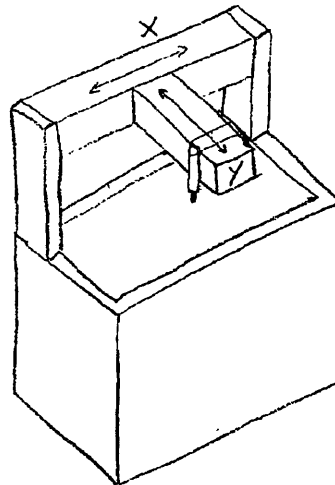


Figure 1.1 Sketch of Concept One

ator systems, one for each axis. However, it results in the nozzle being held by a cantilever arm, resulting in a vertical deflection at the nozzle tip as well as a moment load on the bearings supporting the y-axis.

The moment load on the bearing is calculated using Equation 1.1.

$$\Sigma M_b = \Sigma(Fd) \quad (1.1)$$

Where M_b is the moment load on the bearing, F is the force, or in this case, the weight of the nozzle and structural member, and d is the distance of the load from the bearing.

In the calculations, there need to be two terms in the right side of the equation. The first F term is the weight of the arm itself and the second is the weight of the nozzle. Both are 4.54 kg (10 lbs). The distance term for the weight of the arm is 330.2 mm (13 inches), half the arm length, and 660.4 mm (26 inches) for the weight of the nozzle, at the tip of the arm for its worst case effect. This calculation is carried out in equation 1.2 and yields 44 Nm (390 lb in).

$$\Sigma M_b = (10 \times 13) + (10 \times 26) = 390lb \cdot in \quad (1.2)$$

The deflection at the end of the beam (worst case nozzle position) is calculated using Equation 1.3.

$$\delta = \frac{FL^3}{3IE} \quad (1.3)$$

where δ is the deflection, F is force, L is length, I is moment of inertia, and E is the Young's Modulus of the material, in this case aluminum. The cross-section of the structural members is taken into account in the calculation of the moment of inertia using Equation 1.4

$$I = \frac{bh^3}{12} \quad (1.4)$$

where b is base and h is height. In this case, both are 152.4 mm (6 inches). The moment of inertia is calculated to be 108 in^4 . The deflection calculation is done according to equation 1.5 and the result is a deflection of 6.76 e-3 mm (2.66 e-4 in).

$$\delta = \frac{15 \times 26^3}{3 \times 108 \times 10e6} = 2.66e - 4in \quad (1.5)$$

1.2.2 Concept Two

Concept Two eliminates the cantilever arm in concept one by having the entire x-axis and nozzle travel back and forth to create the y-axis. Actuators and linear motion systems are required along both sides of the table as well as along the x-axis. This concept is sketched

in Figure 1.2. Right off, this concept eliminates the cantilever, so there is no deflection at

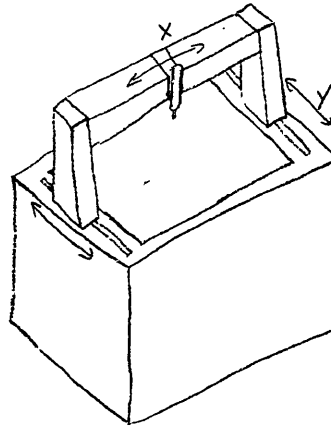


Figure 1.2 Sketch of Concept Two

the end of the beam or a moment load at the bearings. However, this concept requires an extra set of linear motion system and actuator, or a complex coupled actuator system. Since the cost of the linear motion systems is a significant part of the total cost of the machine, this concept becomes too expensive compared to concept one. Additionally, this concept requires extensive sealing of the two rail systems since they are at the same level with the table and would be exposed to a lot of water and abrasive spray. This design would also eliminate the possibility of cutting any parts longer than the table as the nozzle needs to travel back and forth along the sides.

1.2.3 Concept Three

Concept Three is a variation on concept two in that the rail system is located at the back of the tank. Only one linear motion system is used for the each axis and the nozzle is extended and retracted over the workspace creating a cantilever arm. This concept is sketched in Figure 1.3. Like concept one, it has a maximum deflection of $6.76 \text{ e-}3 \text{ mm}$ ($2.66 \text{ e-}4 \text{ in}$) and a moment load on the bearings of 44 Nm (390 lb in) since it has the same

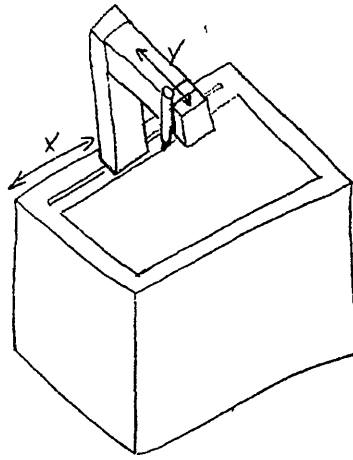


Figure 1.3 Sketch of Concept Three

arm dimensions. Same as concept one, this one only uses one set of motion system per axes, making it an attractive choice. However, as with concept two, one of the axes is on the same level as the tank and therefore exposed to a harsh environment of water and abrasive, making it hard to seal.

1.2.4 Concept Four

Concept Four uses a rotating arm suspended from its center by a frame straddling the center of the table. The nozzle traverses the rotating arm creating an $R-\theta$ system of motion. Figure 1.4 is the sketch of this $R-\theta$ concept. This concept shortens the length of the cantilever arm compared to concept one and three. In addition, the shortened cantilever section is counterbalanced by the similar arm section on the other side, thus reducing the moment load felt by the bearing. This system would use one linear motion system and one rotary motion system. Though this concept seems like a good idea at first glance, it has some inherent problems associated with it. The nozzle would have to travel under the frame, which would make it impossible to seal that axis with a bellows. Secondly, it would make it difficult for the water and abrasive lines to follow the nozzle back and forth under the

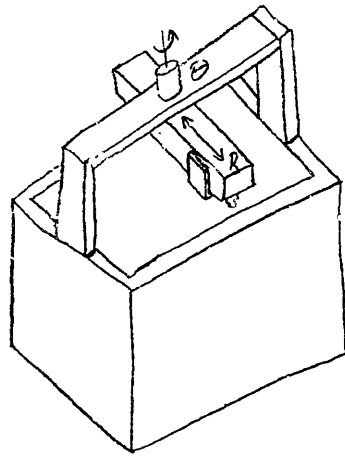


Figure 1.4 Sketch of Concept Four

straddling frame. Lastly, this design would prohibit the cutting of materials longer than the tank width, as the material could not extend beyond the sides due to the straddling frame.

1.2.5 Concept Five

Concept Five, sketched in Figure 1.5, is similar to four except that what used to be the rotating arm now traverses the central frame, creating an X-Y system.

This concept has all the advantages of concept four, but all the disadvantages as well. For this reason, upon closer examination, it is not a feasible design.

1.2.6 Concept Six

Concept Six is a θ - θ system. It is sketched in Figure 1.6. One post is attached at the center back of the tank and a cantilevered arm is split into two even length sections. Two rotating joints, one at the attachment point of the cantilever arm and the second at the split of the arm, position the nozzle anywhere over the workspace.

Since the arm needs to reach the corner of the work area, the arm needs to be slightly longer than with any of the X-Y concepts. Therefore, the moment load on the bearings and

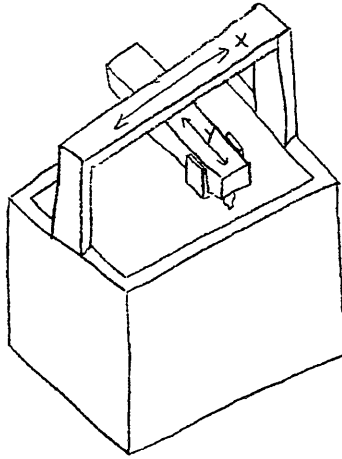


Figure 1.5 Sketch of Concept Five

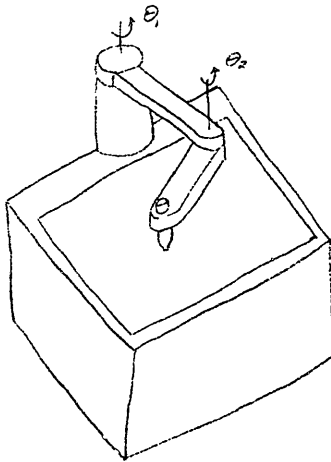


Figure 1.6 Sketch of Concept Six

the maximum deflection and is slightly higher. The moment load was calculated to be 49.7 Nm (440 lb in) using equation 1.1 and the maximum deflection was calculated to be 9.4 E-3 mm (3.70 E-4 in) using equation 1.3.

This is an attractive design because it uses two rotary systems as opposed to linear systems, which eliminates the need for bellows. On the other hand, the controls for such a machine would be more difficult than for an X-Y system.

1.2.7 Concept Seven

Concept Seven is similar to concept three, but instead of the arm traversing along the back of the machine, it rotates at its base thereby creating an R- θ system. Figure 1.7 is a sketch of this system. This R- θ system is more feasible than concept four because the bellows

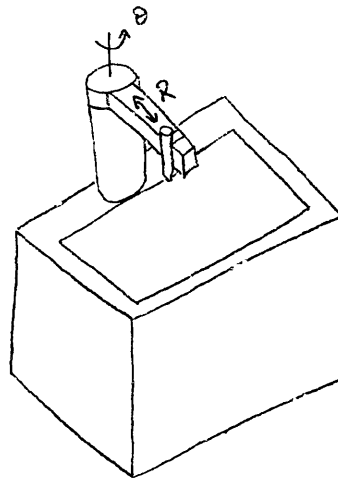


Figure 1.7 Sketch of Concept Seven

and hose problems do not exist here. Like the θ - θ system of concept six, the moment load on the bearings and the maximum deflection were calculated to be 49.7 Nm (440 lb in) and 9.4×10^{-3} mm (3.70×10^{-4} inches) respectively.

This design is attractive because it uses one rotary system and one linear system, keeping the cost down, plus it only requires one set of bellows.

1.3 First Pass Comparison and Elimination

Now that all the generated concepts are introduced, they are compared and a first pass elimination occurs to discard the expensive or otherwise unfeasible ideas. Table 1.1 below is a summary of the concepts and their characteristics.

TABLE 1.1 First Pass Comparison of Concepts

Concept	M_b (lb-in)	Max δ (in)	No. of Bearing Systems	Feasible for Other Reasons
1	390	2.66 e-4	2	Y
2	0	0	3	N
3	390	2.66 e-4	2	N
4	130	2.77 e-5	2	N
5	130	2.77 e-5	2	N
6	440	3.70 e-4	2	Y
7	440	3.70 e-4	2	Y

As can easily be gathered from the table, three concepts emerge; concepts one, six, and seven. These concepts, regardless of the moment loads and deflections produced, are the only feasible designs for various reasons discussed in Section 1.2. These three concepts, X-Y, R- θ and θ - θ are put through further analysis in a second pass comparison and final concept selection.

Chapter 2

CONCEPT SELECTION

Three concepts emerged from a first pass concept comparison. These concepts are referred to in terms of their system of motion. The remaining concepts are the X-Y system, the R- θ system and the θ - θ system. These three concepts were further analyzed and compared in order to ultimately choose the best system for this machine.

2.1 Error Budget

The first step in further analysis of the remaining concepts is the formulation of the error budget. The error budget is a way of keeping track of all the errors created by the different components of a machine, as well as a way of allocating the total permissible error to those components. It is also a design tool to help predict how the final design will behave.

The first step in formulating an error budget is to develop a kinematic model of the proposed machine in the form of a series of homogeneous transformation matrices. The next step is to systematically analyze each type of error that can occur in the system and use the transformation matrices to determine their effect on the toolpoint position accuracy with respect to the workpiece.

2.1.1 The Homogeneous Transformation Matrix Model of the Machine

In order to represent the relative position of a rigid body in three-dimensional space with respect to a given coordinate system, a 4 x 4 matrix is needed. This matrix, called the homogeneous transformation matrix, represents the coordinate transformation to the reference coordinate system from that of the rigid body frame. The first three columns of the matrix are direction cosines (unit vectors i, j, k) representing the orientation of the rigid body's coordinate axes with respect to the reference coordinate system. The last column represents the position of the rigid body's coordinate system's origin with respect to the reference coordinate system. The first three entries in the fourth row are set to 0, and the last entry in the fourth row is a scale factor which is usually set to 1 to avoid confusion. For book-keeping purposes, when defining a transformation matrix, the pre-superscript represents the reference frame you want the result to be represented in, and the post-subscript represents the reference frame you are transferring from. Equation 2.1 shows a sample homogeneous transformation matrix:

$${}^R T_n = \begin{bmatrix} O_{ix} & O_{iy} & O_{iz} & P_x \\ O_{jx} & O_{jy} & O_{jz} & P_y \\ O_{kx} & O_{ky} & O_{kz} & P_z \\ 0 & 0 & 0 & 1 \end{bmatrix} \quad (2.1)$$

It follows then, that the equivalent coordinates of any point in a coordinate frame n , with respect to a reference frame R , are

$$\begin{bmatrix} X_R \\ Y_R \\ Z_R \\ 1 \end{bmatrix} = {}^R T_n \begin{bmatrix} X_n \\ Y_n \\ Z_n \\ 1 \end{bmatrix} \quad (2.2)$$

In this way, machine structures can be decomposed into a series of coordinate transformation matrices which describe the relative position of each axis, starting from the tool tip

and working back to the base reference coordinate system. Once all the transformation matrices are known for each axis, the position of the tool tip with respect to the reference coordinate system is the sequential product of all the transformation matrices. In the case where there are four coordinate systems plus the reference coordinate system, the position of the tooltip with respect to the reference coordinate system would be

$${}^R T_4 = {}^R T_1 {}^1 T_2 {}^2 T_3 {}^3 T_4 \quad (2.3)$$

Since the concepts thus far are not far enough along to call for specific bearing needs, the error analysis will include only errors introduced into the system by deflections of the members due to weight and accelerations.

All rigid bodies inherently have three translational ($\delta_x, \delta_y, \delta_z$) and three rotational ($\epsilon_x, \epsilon_y, \epsilon_z$) error components associated with them. For any given machine member, the error matrix describing its error in position with respect to its ideal position is

$$E = \begin{bmatrix} 1 & -\epsilon_Z & \epsilon_Y & \delta_X \\ \epsilon_Z & 1 & -\epsilon_X & \delta_Y \\ -\epsilon_Y & \epsilon_X & 1 & \delta_Z \\ 0 & 0 & 0 & 1 \end{bmatrix} \quad (2.4)$$

Therefore, the transformation matrix for the same member from one coordinate reference to another is

$${}^R T_n = \begin{bmatrix} 1 & -\epsilon_Z & \epsilon_Y & a + \delta_X \\ \epsilon_Z & 1 & -\epsilon_X & b + \delta_Y \\ -\epsilon_Y & \epsilon_X & 1 & c + \delta_Z \\ 0 & 0 & 0 & 1 \end{bmatrix} \quad (2.5)$$

where a, b, and c are the distances between the two coordinate systems in the X, Y, and Z directions respectively.

Throughout this section of the analysis, several important factors should be pointed out with respect to waterjet cutters. Since the cutting tool is a jet of water, there are no lateral cutting forces that contribute errors in the error budget. In addition, since the toolpoint, does not come in contact with the workpiece, the z-direction (up and down) is not a sensitive direction, meaning that the final error of the toolpoint in the z-direction is not as significant as the x and y direction errors.

2.1.2 X-Y Concept

A simple schematic of the X-Y concept with the required dimensions and motions is shown in Figure 2.1. Note that the shape of the structural members on the schematic is not

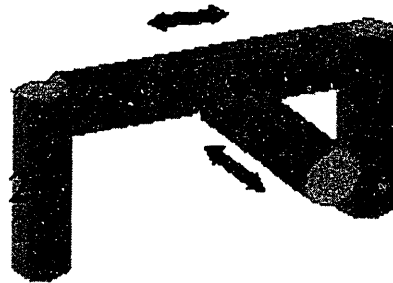


Figure 2.1 Schematic of the X-Y concept

the actual shape analyzed.

Development of Kinematic Model of the Machine

All the concepts are analyzed in their worst-case positions. For the X-Y concept, this position is with the y-axis in the center of the x-axis, and the nozzle all the way out on the cantilever arm. The first concept (as well as the other two), are made up of three structural members plus the nozzle. Therefore, five coordinate systems are needed to kinematically model the machine. The first is the reference coordinate system CSR, the second CS1

(coordinate system one) is the system attached to member one, and so on all the way to CS4, attached to the nozzle. This model is illustrated in Figure 2.2.

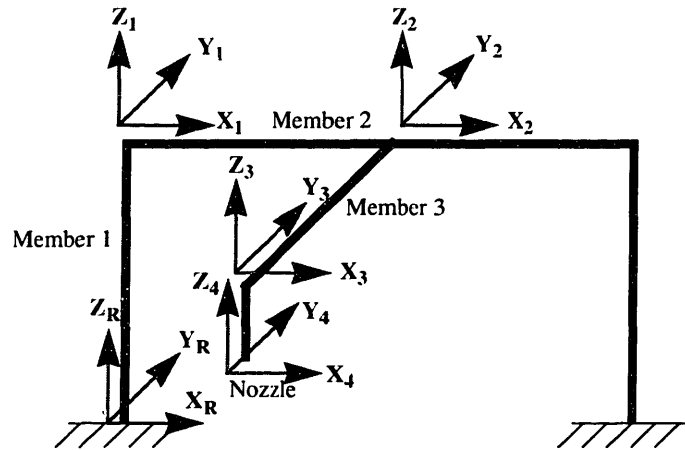


Figure 2.2 Kinematic Model for X-Y Concept

The transformation matrices from each coordinate system to its adjacent coordinate system follows the same format as Equation 2.5. Now, for a tool located at the origin of CS4, the actual coordinates of the toolpoint in the reference coordinate system are given by:

$$\begin{bmatrix} X_t \\ Y_t \\ Z_t \\ 1 \end{bmatrix}_{actual} = {}^R T_4 = {}^R T_1 \cdot {}^1 T_2 \cdot {}^2 T_3 \cdot {}^3 T_4 \quad (2.6)$$

The ideal coordinates of the toolpoint would be the sum of all the individual components along their respective axes:

$$\begin{bmatrix} X_t \\ Y_t \\ Z_t \end{bmatrix}_{ideal} = \begin{bmatrix} a_1 + a_2 + a_3 + a_4 \\ b_1 + b_2 + b_3 + b_4 \\ c_1 + c_2 + c_3 + c_4 \end{bmatrix} \quad (2.7)$$

The translational errors in the tip of the nozzle are thus given by:

$$\begin{bmatrix} \delta_{xt} \\ \delta_{yt} \\ \delta_{zt} \end{bmatrix} = \begin{bmatrix} X_t \\ Y_t \\ Z_t \end{bmatrix}_{actual} - \begin{bmatrix} X_t \\ Y_t \\ Z_t \end{bmatrix}_{ideal} \quad (2.8)$$

Mathcad was used to symbolically evaluate Equation 2.8 which incorporates Equations 2.6 and 2.7. Second order terms are neglected. The result is Equation 2.9.

$$\begin{bmatrix} \delta_{xt} \\ \delta_{yt} \\ \delta_{zt} \end{bmatrix} = \begin{bmatrix} E \\ F \\ G \end{bmatrix} \quad (2.9)$$

$$\text{Where } E = \delta_{x1} + \delta_{x2} + \delta_{x3} + \delta_{x4} + \epsilon_{y2} \cdot c_4 + \epsilon_{y1} \cdot c_3 + \epsilon_{y2} \cdot c_3 - \epsilon_{z1} \cdot b_3 - \epsilon_{z3} \cdot b_4 \\ + \epsilon_{y3} \cdot c_4 - \epsilon_{z2} \cdot b_3 - \epsilon_{z1} \cdot b_4 - \epsilon_{z1} \cdot b_2 + \epsilon_{y1} \cdot c_2 - \epsilon_{z2} \cdot b_4 + \epsilon_{y1} \cdot c_4$$

$$F = \delta_{y1} + \delta_{y2} + \delta_{y3} + \delta_{y4} + \epsilon_{z1} \cdot a_3 + \epsilon_{z2} \cdot a_4 - \epsilon_{x2} \cdot c_4 - \epsilon_{x2} \cdot c_3 - \epsilon_{x1} \cdot c_4 \\ - \epsilon_{x1} \cdot c_3 - \epsilon_{x1} \cdot c_2 + \epsilon_{z1} \cdot a_2 + \epsilon_{z2} \cdot a_3 - \epsilon_{x3} \cdot c_4 + \epsilon_{z3} \cdot a_4 + \epsilon_{z1} \cdot a_4$$

$$G = \delta_{z1} + \delta_{z2} + \delta_{z3} + \delta_{z4} + \epsilon_{x2} \cdot b_4 - \epsilon_{y1} \cdot a_2 - \epsilon_{y2} \cdot a_4 - \epsilon_{y1} \cdot a_4 - \epsilon_{y2} \cdot a_3 \\ + \epsilon_{x1} \cdot b_3 + \epsilon_{x1} \cdot b_4 + \epsilon_{x2} \cdot b_3 + \epsilon_{x3} \cdot b_4 - \epsilon_{y3} \cdot a_4 + \epsilon_{x1} \cdot b_2 - \epsilon_{y1} \cdot a_3$$

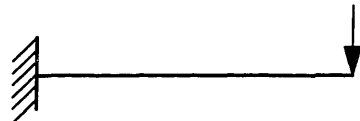
The error gains are the coefficients associated with each of the δ and ϵ errors above. Note that the translational error gains are unity. It is the angular errors which can have potentially large gains associated with them. These error gains, called Abbe effects are most often the dominant errors in a machine.

Analysis of Error Sources


As mentioned before, only deflection errors due to weight and acceleration will be analyzed here so that the concepts can be compared solely on a structural basis. A free body diagram of each structural members is drawn and all weight and acceleration forces are applied to it. All resulting deflections and rotations are then calculated and added to a specially designed spreadsheet so that a final nozzle tip error can be calculated taking into

account all possible structural deflections. Figure 2.4 shows an example of all the calculated deflections and rotations for each of the structural members in the X-Y concept.

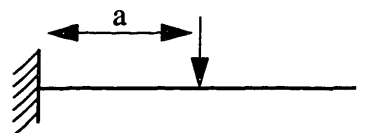
The following equations for the respective sketched boundary conditions were used to calculate the deflections and rotations on each member.



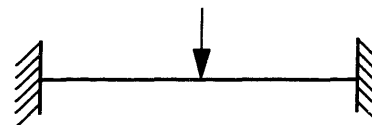
$$\delta = \frac{Fl^3}{3IE}, \theta = \frac{Fl^2}{2IE} \quad (2.10)$$



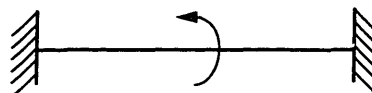
$$\delta = \frac{Ml^2}{2IE}, \theta = \frac{Ml}{IE} \quad (2.11)$$



$$\delta = \frac{Fa^2(a-3l)}{6IE}, \theta = \frac{Fa^2}{2IE} \quad (2.12)$$



$$\delta = \frac{Fl^3}{192IE} \quad (2.13)$$



$$\theta = \frac{Ml}{12IE} \quad (2.14)$$

Tension and Compression $\delta = \frac{Fl}{AE} \quad (2.15)$

Torsion $\theta = \frac{Tl}{GJ} \quad (2.16)$

The error budget spreadsheet is set up so that the designer can input the dimensions and cross-sectional shape of each of the three structural components of the machine separately, as well as if the member is solid or hollow. An example input window is Figure 2.3

Member 2 (cross-bar)

solid <= Solid or Tube
square <= Circle or Square

<i>Circle</i>			
OD:	6	in	
ID:	5	in	

<i>Square</i>			
Width	2	in	
Height	2	in	
Thickness	0.5	in	

length (in)	45	in	
-------------	----	----	--

2nd Moment of Intertia (I)	1.33	in ⁴	
Polar Moment of Intertia (J)	2.67	in ⁴	
X-sec Area	4.00	in ²	
Volume	180.00	in ³	
Weight	51.12	lb	

Figure 2.3 Example Member Shape and Dimension Input Window

Then, based on these dimensions and cross-sections, the error calculations are carried out and the final translational errors at the tip of the nozzle are displayed. Figure 2.4 and

Error calculations

Member 1, CS1 δ (in) / ϵ (rad)	Member 2, CS2 δ (in) / ϵ (rad)	Member 3, CS3 δ (in) / ϵ (rad)
δ , y, torsion M mem3	δ , z, weight nozzle	δ , z, weight nozzle
1.15E-05	-1.23E-04	-6.90E-04
δ , x, accel n+a	δ , y, accel nozzle	δ , x, accel nozzle
3.00E-06	1.23E-05	6.90E-05
δ , y, accel n	δ , x, compr accel n+a	δ , x, accel arm
9.17E-07	6.35E-07	4.90E-05
δ , x, react M W nozzle	ϵ , x, torsion M mem3	ϵ , x, weight nozzle (rad)
6.45E-06	1.51E-04	5.17E-05
ϵ , x, torsion M mem3	ϵ , z, M accel n+a	ϵ , z, accel nozzle (rad)
9.55E-07	4.14E-06	5.17E-06
ϵ , x, accel nozzle		ϵ , z, accel (rad)
5.73E-08		1.96E-06
ϵ , y, accel n+a		
1.87E-07		
ϵ , y, react M W nozzle	moment, weight nozzle	
5.37E-07	2.00E+02	

Figure 2.4 Example Error Calculation Segment of Spreadsheet

Figure 2.5 show spreadsheet outputs.

For a consistent comparison, the member lengths are set to just meet the requirements for a 26 inch x 26 inch servo-able area. The length of the posts is set at 24 inches. All the

Error at Nozzle Tip (in)	
δ_{xt}	0.000205
δ_{yt}	0.001652
δ_{zt}	-0.003862

Figure 2.5 Example Error at Tip Display Segment of Spreadsheet

members are given a square cross-section of 6 inches x 6 inches and a 1-inch wall thickness and are given the material properties of aluminum. The acceleration used to calculate deflections is 0.1 g's, the maximum acceleration originally specified in the list of functional requirements.

For the X-Y concept, the x-axis of the machine needs to be approximately 40 inches long to allow for the 26-inch required travel and the space required for the compressed bellows. Similarly, the length of the y-axis would also have to be 40 inches. With these lengths, and the other dimensions discussed above, the final position errors at the nozzle come out to $\delta_x = 0.00010$ inches, $\delta_y = 0.00015$ inches, and $\delta_z = 0.00055$ inches. Since the z direction is not a sensitive direction, a resultant error offset was calculated for the x and y direction errors. This came out to 0.00018 inches.

The stiffnesses of the different members was also calculated by dividing the force applied to the member by the resulting deflection in the member. This stiffness is dependent of the geometry of the members and is a good way of comparing the concepts and to understand why the magnitudes of the deflections come out to what they do. Member one turns out to have a stiffness of $7.0 \text{ e}+5$ lb/in. Members two and three have stiffnesses of $4.9 \text{ e}+6$ and $7.6 \text{ e}+4$ lb/in respectively

2.1.3 R- θ Concept

Figure 2.6 shows a simple schematic of the R- θ concept. As with the X-Y concept, the shapes of the structural members on the schematic do not correspond to the actual shapes analyzed in the error budget spreadsheet.

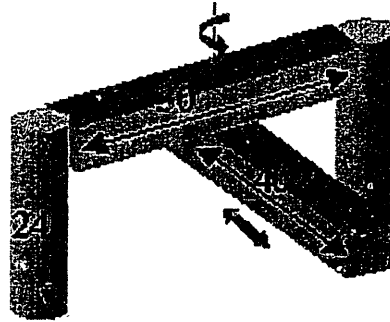


Figure 2.6 Schematic of the R- θ Concept

Development of Kinematic Model of the Machine

The worst case position of the R- θ concept puts it in a position very similar to that of the X-Y concept. Therefore, the kinematic model of the machine is basically the same as for the X-Y concept, except that some of the member dimensions are different. So for all practical purposes, Figure 2.2 is a good schematic of the kinematic model for this concept as well.

In addition to the kinematic model, the transformation matrices follow the same format as shown in Equations 2.6 through 2.9. Since the worst-case positions of the two machines are the same in both cases, the final structural error matrices are identical.

Analysis of Error Sources

The same procedure was followed in analyzing the sources of error for this concept as for the previous concept. Equations 2.10 through 2.16 were utilized to apply weight and acceleration forces to the different members of the structure and calculate deflections and rotational errors. The information was again entered into the error budget spreadsheet which allows the designer to specify member dimensions and other properties.

All the member cross-sections were left as previously described to maintain consistency between concept analyses. As with the first concept, the post lengths were set to 24 inches to maintain continuity. However, the other members were given different lengths. Mem-

ber 2 in this concept was set to 30 inches since the working area still had to be straddled, yet the member length did not have to accommodate bellows or ballscrew assemblies. Similarly, member 3 was given a length of 42 inches since it still had to accommodate bellows and a ballscrew, plus it had to be a little longer since it had to reach the corner of the 26 inch by 26 inch work area from its pivot point at the center of member 2. Once these dimensions were entered into the spreadsheet, the errors at the nozzle tip were calculated to be $\delta_x = 0.00011$ inches, $\delta_y = 0.00014$ inches, and $\delta_z = 0.00051$ inches. In this case, the resultant error in the x and y directions also came out to 0.00018 in. Coincidentally, with the shortening of one member and the lengthening the other, the same resultant error was achieved. The member stiffnesses are $7.0 \text{ e}+5$, $1.2 \text{ e} +7$, and $6.6 \text{ e}+4$ lb/in for members 1, 2, and 3 respectively.

2.1.4 θ - θ Concept

The θ - θ concept is considerably different from the previous concepts. It is composed of

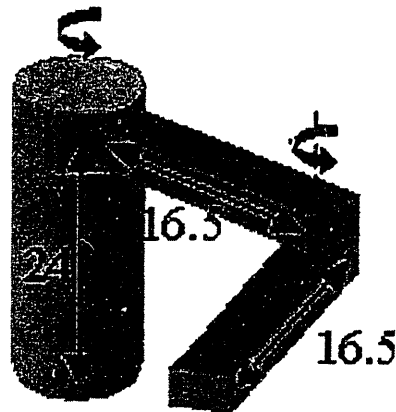


Figure 2.7 Schematic of the θ - θ Concept

only one post, and segmented arm with a shoulder joint and an elbow joint. Figure 2.7

shows a simple schematic of this concept. Once again, the shape of the members depicted in the schematic are not the actual shapes analyzed.

Development of Kinematic Model of the Machine

The structure of this model is somewhat different than the previous concepts discussed. The worst-case position of this model is simply with the elbow joint straight. Five coordinate systems are still needed so that each member has its own coordinate system associated with it. Since this structure is going to be analyzed with a straight elbow joint, four coordinate systems could theoretically be sufficient, however, to maintain both flexibility and continuity, five coordinate systems were used. Figure 2.8 shows the kinematic model

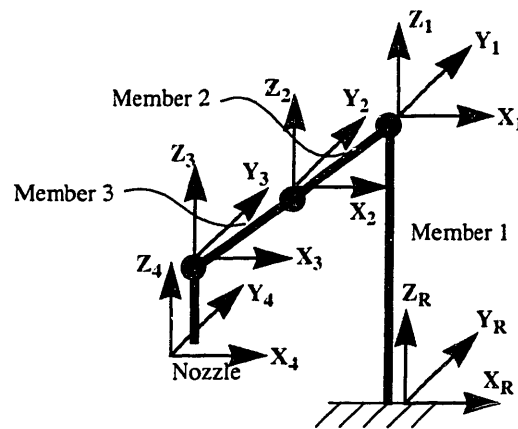


Figure 2.8 Kinematic Model for θ - θ concept

for this concept. Since continuity was maintained, and five coordinate systems were used, the transformation matrices have the same structure as the previous concepts. Therefore, Equations 2.6 through 2.9 still apply.

Analysis of Error Sources

Unlike the first two concepts discussed, the structural error analysis on this one was a little different. Equations 2.10 through 2.16 were still applied to the different members, how-

ever, in this case the members were oriented differently. For this reason, a whole new set of force-induced deflection and rotations had to be analyzed, calculated, and combined to create all the possible deflection errors.

The length of the post was set at 24 inches and the length of each segment of the arm was set to 16.5 inches. This length would allow the arm to extend from the position of the post to the corner of the work area. Once these dimensions were entered into the spreadsheet, the nozzle tip errors were calculated to be $\delta_x = 0.00018$ inches, $\delta_y = 0.00036$ inches, and $\delta_z = 0.00233$ inches. The x-y resultant deflection was 0.00032. Member one had a stiffness of $3.5 \text{ e}+5$ lb/in while members two and three were both $1.1 \text{ e}+6$ lb/in.

The resultant error at the tip of the nozzle was almost double for this concept that for the other two. The source of this error can also be seen in the stiffness of member one. It was half as stiff as member one of each of the other concepts. The reason for this is that the previous two concepts were splitting up all the applied forces between two posts, where only one post was taking all the forces in this case. For this reason, the deflections in the post were doubled.

2.2 Concept Comparison

Now that the structural behaviors of the concepts are known, other aspects need to be explored. Among these are the difficulty and cost of accomplishing the specified functional requirements such as maximum acceleration, minimum resolution requirements, complexity of controls and cost of motion components.

One of the functional requirements on this machine was the need for a maximum acceleration of .1 g's, or 3.2 ft/s^2 ($.98 \text{ m/s}^2$). An acceleration of this magnitude would be relatively easy to accomplish with an X-Y system. However, with an R- θ system, such accelerations would become tougher to achieve as the nozzle approaches the pivot point of the arm. In order for the nozzle to accelerate at rate of .1 g's in a tangential direction at its closest point to the pivot point, the opposite end of the arm would have to be accelerating

approximately 5 times as fast, or around .5 g's. For this reason, this concept does not perform very well in terms of meeting this requirement. The forces generated would be much greater than those calculated in the error budget, hence the error at the tool tip would be much greater as well. The θ - θ concept has similar issues. When the relative angles of the two arms are at their extremes, either very small or very large, similar acceleration singularities are going to occur. This is one of the weaknesses of the two θ designs.

Along the same lines, minimum resolution requirements will be more difficult to adhere to with the angular motion designs. Since both of the latter designs have use angular motion of one or more arms, small motions at the pivot point(s), get amplified by the length of the arm(s). Therefore, much finer, and consequently more expensive, actuators need to be used. The X-Y design however, does not have these drawbacks because the axes are decoupled.

Complexity of the controls also increases with the angular motion systems. Where it is relatively simple to control the nozzle position on an X-Y table due to its decoupled nature, it is increasingly more difficult as you move from R- θ to θ - θ systems of motion for the opposite reason. In both of the angular motion systems, the motion of all the degrees of freedom are coupled. Additionally, in most circumstances for both angular systems, the velocity of the actuators needs to vary even when the velocity of the nozzle needs to remain constant. This factor in itself creates much complexity in the controls of the two θ systems.

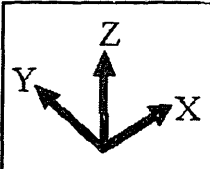
For the same reasons discussed above, the cost of the systems would increase with the angular motion systems. In order to adhere to the resolution requirements, the motion actuators for the angular systems would need to be much more sophisticated versus a relatively simple system for the X-Y table. Likewise, the controls aspect of the θ systems would require more time and more sophisticated equipment and therefore be more expensive than the X-Y system.

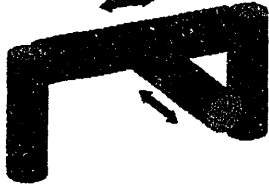
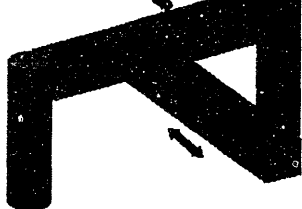
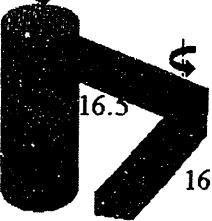
2.3 Summary and Conclusion

Table 2.1 is a comprehensive summary of the comparison of the X-Y, R- θ , and θ - θ concepts. It lists the results of the error budget, the member stiffnesses, and the summary of the functional requirement discussion.

The error budget results do not show an advantage between the first two concepts, however, it does show that the θ - θ concept does worse than the other two. However, the functional requirement comparison does point out the weaknesses of the two angular motion concepts versus the X-Y table. For these reasons, the X-Y concept is the better choice for the design of the small waterjet cutter.

TABLE 2.1 Summary Table of Error Budget and Concept Comparison

Reference
Coordinate System


X-Y Concept		R-θ Concept		θ-θ Concept	
					
Error at Nozzle Tip: (in)		Error at Nozzle Tip: (in)		Error at Nozzle Tip: (in)	
δ_{xt}	0.00010	δ_{xt}	0.00011	δ_{xt}	0.00018
δ_{yt}	0.00015	δ_{yt}	0.00014	δ_{yt}	-0.00026
δ_{zt}	-0.00055	δ_{zt}	-0.00051	δ_{zt}	-0.00233
$\delta_{result(x,y)}$	0.00018	$\delta_{result(x,y)}$	0.00018	$\delta_{result(x,y)}$	0.00032
Member Stiffnesses (lb/in)		Member Stiffnesses (lb/in)		Member Stiffnesses (lb/in)	
Member 1	7.0E+05	Member 1	7.0E+05	Member 1	3.5E+05
Member 2	4.9E+06	Member 2	1.2E+07	Member 2	1.1E+06
Member 3	7.6E+04	Member 3	6.6E+04	Member 3	1.1E+06
Sensitive Directions x,y					
Functional Requirements:	X-Y Concept	R-θ Concept	θ-θ Concept		
26 in sqr machinable area	need axes lengths 40 in X axis 40 in Y axis	need axes lengths 30 in X axis 42 in Y axis	need axes lengths 2 - 16.5 in arms		
Max accel of .1 g's	easy to accomplish with this design	difficult when carriage is close to pivot point	difficult when angles are at extremes		
Min resolution of .0005 in/step	least expensive actuators + controls	mid expensive actuators + controls	most expensive actuators + controls		
Table, arm, controls < \$10 k Most significant components	2 ballscrews 2 linear bearing/rails	1 ballscrew, 1 linear bearing/rail, 1 rotary bearing	3 rotary bearings		

Chapter 3

X-Y CONCEPT PRELIMINARY DESIGN

Once the X-Y concept was chosen as the system of motion for the small waterjet cutter, preliminary design steps began. Several different structural cross-sections were considered. Of the more feasible designs, two were analyzed further to determine the optimal cross-section to maximize the stiffness of the system while minimizing the size of the required bellows, which must surround and seal the entire axis to protect it from the harsh working environment of an abrasive waterjet cutter. In addition, finite element analysis (FEA) models of the considered structures were used to determine their frequency response behavior.

In the midst of these analyses, the novel idea of using solely the linear rails as the structure of the machine sparked a change in the functional requirements of the machine so that this design could be pursued.

3.1 Optimal Structural Cross-Section

3.1.1 Maximization of Torsional Stiffness

Since torsion is a dominant mode in the x-axis of the current X-Y design (due to the catil-
evered y-axis), the goal here was to maximize the torsional stiffness while minimizing the diameter of the circle required to enclose the cross-section. Several cross-sections for the x-axis of the small waterjet machine were considered and the two most feasible ones, a

rectangular beam, and a C-channel beam, were then compared further. The idea was that the C-channel would allow the rail and truck to be nested within the beam, therefore minimizing the diameter of the bellows required to cover the assembly, while still maintaining a comparable torsional stiffness to that of the rectangular beam. Both beam types were modeled with size 55 linear guide rails and the corresponding truck.

The two beams were compared using a spreadsheet specially created which calculates the bellows size requirements for any size beam cross-section. All of the dimensions of the beams, except those driven by other parts in the assembly, are entered into the spreadsheet by the designer. Then, the spreadsheet plots the beams plus the other needed components and then the bellows size needed to surround all the components. It also calculates the moment of inertia, the cross-sectional area of the beams, and the torsional stiffness of the beam cross-sections in order to aid in the comparison and selection. The spreadsheet uses the material properties of steel, as it was determined that steel was a better choice than aluminum for the material of the structure since it is relatively inexpensive and has better structural characteristics.

The spreadsheet was used to find the dimensions of the two beams that would yield approximately a 10-inch diameter bellows and simultaneously maximize the torsional stiffness of the axis assembly. Figure 3.1 shows a snapshot of the spreadsheet showing the dimensions of the two beam types and the resulting characteristics. The results indicate that the better cross-section would be the 3 in x 6 in rectangular steel tube with 0.5-inch wall thickness. While both cross-sections would require the same size bellows, the rectangular section is almost 35 times stiffer in torsion than the C-channel. In addition, when compared to the solid beam of same outside dimensions, the cross-sectional area dramatically increases while the moment and the torsional stiffness improve only slightly. The increase in weight and cost of material outweighs the small improvement in the other design parameters.

Bellows Diameter Comparison

Units: in in or mm

Rectangular Beam

Beam Height	3.000	in
Beam Width	6.000	in
Thickness	0.500	in
Tot. Bearing Height	3.125	in
Tot. Bearing Width	5.500	in
Y Axis Height	2.000	in
Y Axis Width	5.500	in

C-Channel

Beam Height (Calculated)	5.500	in
Beam Width	7.000	in
Thickness	0.500	in
Tot. Bearing Height	3.125	in
Tot. Bearing Width	5.500	in
Min. Straddle Height (Calculated)	2.000	in
Straddle Width	5.000	in
Y Axis Height	2.000	in
Y Axis Width	5.500	in
Gap Between Bottom of Beam and Top of Y Axis	0.125	in

	Moment of Inertia		Xsect Area	Torsional Stiffness	Bellows Diameter	Cost		
	Ix	Iy				Bellows	Beam	Straddle
Rectangular	167.0	67.0	8.00	6.6E+06	9.959	Same	Aprx Same	N/A
C-Channel	121.5	137.2	8.50	1.9E+05	9.907	Same	Aprx Same	Extra

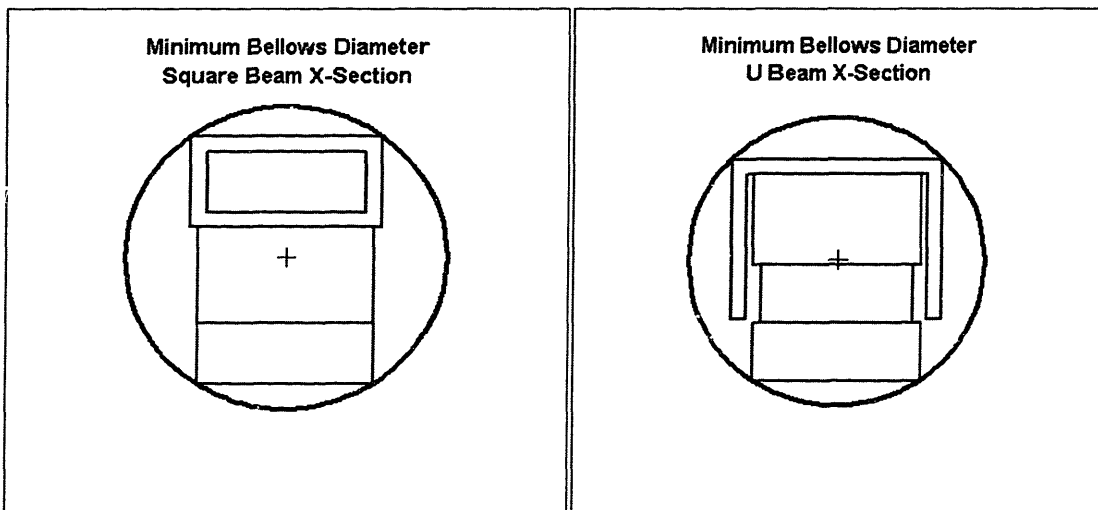


Figure 3.1 Bellows Diameter Spreadsheet Comparison of Results

3.1.2 Finite Element Analysis

Once these dimensions were established, solid models were created on Pro/ENGINEER and FEA analysis was run on Pro/Mechanica in order to find the first two mode frequen-

cies of the structures. Several different iterations were run with various parameters such as one vs. two size 55 ball bearing trucks and a consistent vs. a tapered y-axis. All the y-axes were modeled as a flat base structure with a size 35 linear guide rail bolted to it and the corresponding truck running on the rail. Additionally, all the models include a 5.79 kg (12.75 lb) block of steel to simulate the weight of the nozzle and its components. A 5.79 kg weight was chosen because that is the weight of a plate that is readily available for testing the bench-level prototype. Figure 3.2 and Figure 3.3 show the solid models of each

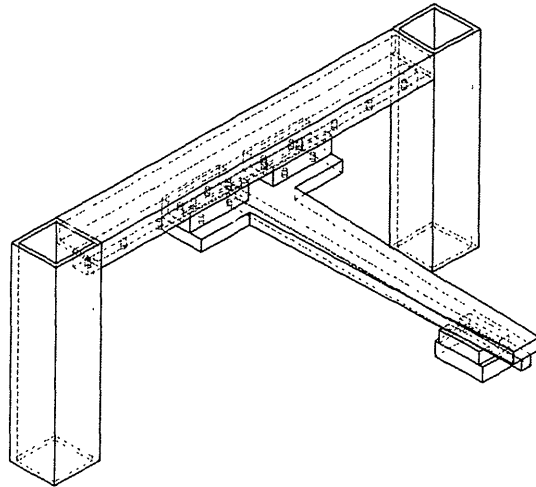


Figure 3.2 Solid Model of Rectangular X-axis

beam type created in Pro/ENGINEER and used to do the finite element analyses.

In order to approximate the stiffness of the bearings in the finite element model, the trucks were assigned a Modulus of Elasticity equal to $1/30^{\text{th}}$ that of steel as in Equation 3.1. This modulus yields equal vertical deflections, i.e., when the truck is loaded vertically, this modulus yields a deflection equal to that listed in the catalog for size 55 trucks. This equivalent modulus is 6897 N/mm^2 ($1.0 \text{ e } 6 \text{ psi}$).

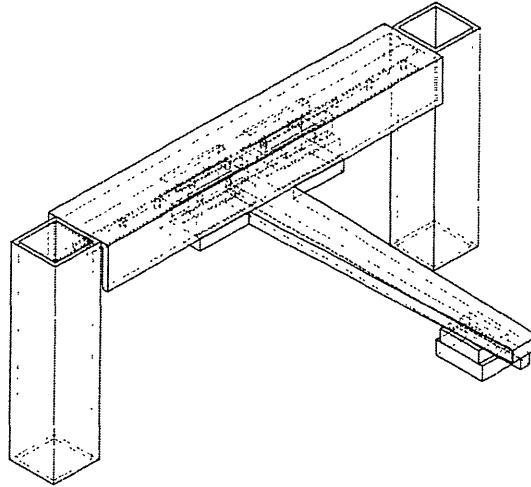


Figure 3.3 Solid Model of C-channel X-axis

$$E_{Truck} = \frac{E_{Steel}}{30} \approx 1 \times 10^6 \text{ psi} \quad (3.1)$$

For this machine to be controllable in an efficient and timely manner, a first natural frequency above 30 Hz is desired. Natural frequencies below this could be excited by the control mechanism or by machine movements or cutting operations.

For all the cases, the first mode shape is a vertical oscillation of the cantilevered y-axis and torsion in the x-axis. The second mode shape is the lateral oscillation of the cantilevered member and bending in the x-axis. Table 3.1 shows the results of the finite element analyses run using the different cross-section configurations.

TABLE 3.1 Summary of FEA Modal Results, Rectangular vs. C-channel

	Dimensions (in)		Mode Frequencies (Hz)			
			1 Carriage		2 Carriages	
	Outside	Wall	1st	2nd	1st	2nd
Rectangular	6x3	0.5 thick	22	50	31	80
Rectangular	6x3	Solid	24	53	35	77
C-Channel	7x5.5	0.5 thick	20	48	26	71

The rectangular cross-section behaves better than the C-channel section since the FEA predicted natural frequencies are higher. However, in the case of the rectangular cross-

section, a second truck is required to bring the first natural frequency to an acceptable level. For the case of the C-channel, not even the second truck yields an acceptable frequency response. Therefore, once again the rectangular beam cross-section proves to be the better choice for the base structure of the x-axis. Here again, the increased weight and cost of making the rectangular beam solid is not justified by the slight increase in the first mode frequency.

Once verifying, using FEA, the previous results that the best cross-section is the 3x6 in rectangular steel tube with 0.5-inch wall thickness, further analysis was done to determine how the same cross-section turned 90 degrees would behave dynamically. This cross-section would have the same diameter bellows requirement, but would have the carriages traversing on the side of the beam as opposed to the bottom, as seen in Figure 3.4. The Pro/

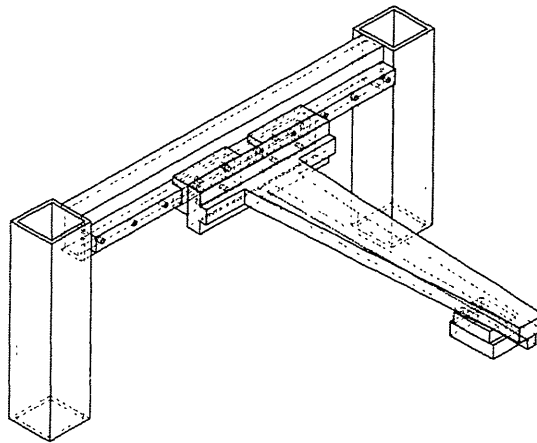


Figure 3.4 Solid Model of Rectangular X-axis Oriented Vertically

Mechanica modal analysis returned the first and second mode frequencies as 26 and 72 Hz respectively. Compared to the horizontal beam placement illustrated in Figure 3.2, the two modes shifted down considerably and below an acceptable level. Therefore, the optimal cross-section is the 3x6 in rectangular steel tube with 0.5-inch wall thickness assembled with the trucks running along the bottom (or top) of the rail.

3.2 Conception of Rails-Only Structure

In the midst of running all the finite element analyses, the novel idea of using just the linear guide rails as the structure of the machine was conceived. Several more FEA analyses were run to test the feasibility of this idea. After running the modal analysis of the structure with just the rails, it was determined that the frequencies were too low for the idea to work with the current dimensions. The concept was so attractive however, that the original functional requirement of the machine were reconsidered. It was decided that the machine would still meet all of its requirements and intended uses if it had a working area of 26 inches by 13 inches (instead of the original 26 by 26 inches). This cuts the length of the cantilevered y-axis almost in half and brings the concept of using the linear guide rails as the structure into the feasible design realm.

3.2.1 Analysis of Bare-Rail Design

Upon the conception of the bare-rail design, several solid models were created to test the validity of the idea. The y-axis was shortened to yield a travel length of 13 inches. Figure 3.5 was the first iteration, taking some of the design from the previous models, including the tapered y-axis base structure. The FEA analysis predicted a first mode at 50 Hz. The mode shape and frequency for the first mode is illustrated in Figure 3.6. As before, the shape of the first mode is a vertical oscillation of the y-axis and torsion in the x-axis while the second mode is a lateral oscillation of the y-axis and bending in the x-axis.

For these new bare-rail concepts, the error budget spreadsheet was revisited. The new dimensions for the structure were input into the spreadsheet in order to make sure that the deflections due to weight and accelerations were not going to be too large. For the structure in Figure 3.5, the δ_x , δ_y , and δ_z errors at the nozzle tip were calculated to be 0.00026, 0.00218, and 0.00531 inches respectively.

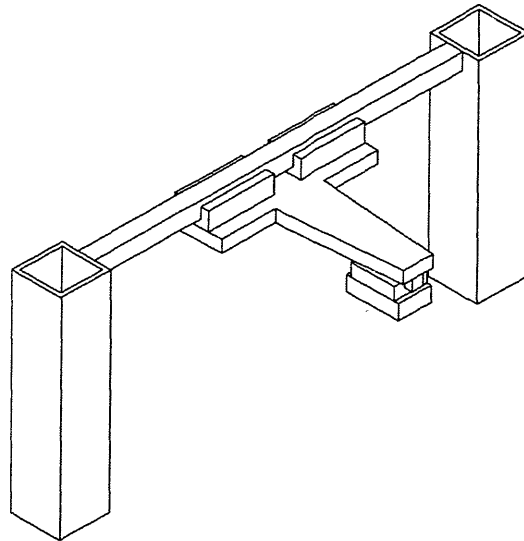


Figure 3.5 Solid Model of Size 55 Bare Rail as X-Axis

Displacement Mag
Deformed Original Model
Max Disp +1.0000E+00
Scale 5.7000E+00
Mode 1, +5.0479E+01

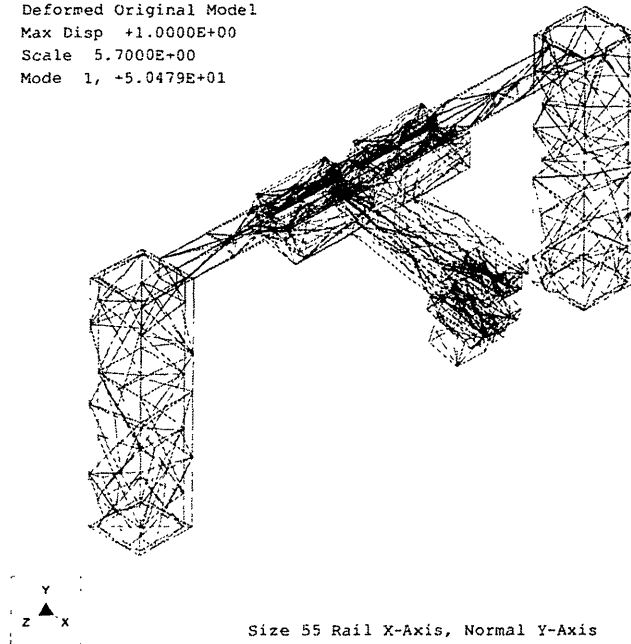


Figure 3.6 FEA Results for Bare Rail as X-Axis

Since this first iteration showed positive results, a second analysis was run, removing the

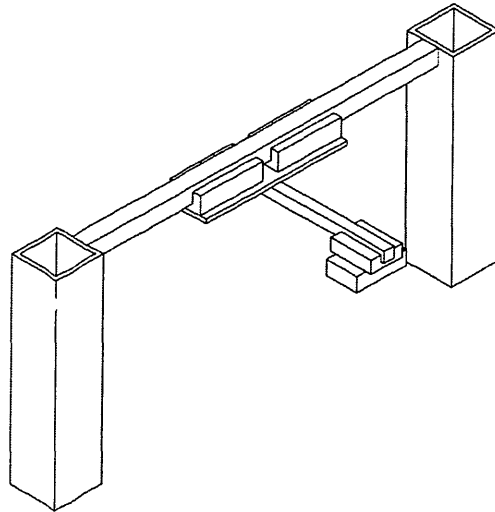
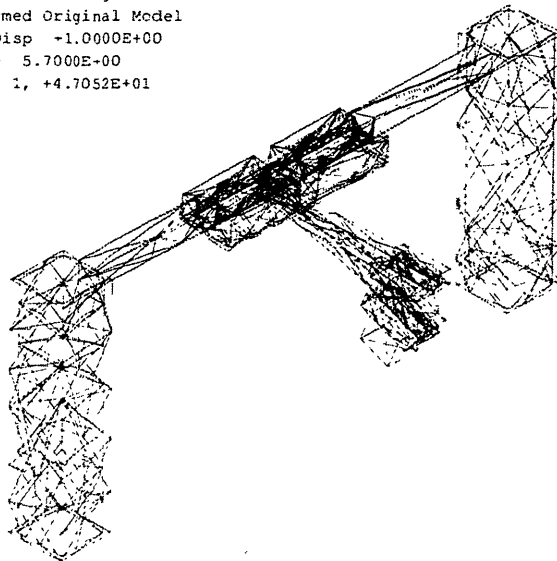


Figure 3.7 Solid Model of Size 55 Rail X-Axis and Size 35 Rail Y-Axis

Displacement Mag
 Deformed Original Model
 Max Disp +1.0000E+00
 Scale 5.7000E+00
 Mode 1, +4.7052E+01



Size 55 Rail X-Axis, Size 35 Rail Y-Axis

Figure 3.8 FEA Results for Size 55 Rail X-Axis and Size 35 Rail Y-Axis

tapered y-axis base feature and only leaving the size 35 linear guide rail. Figure 3.7 shows the solid model and Figure 3.8 shows the FEA results. The first mode was calculated to be 47 Hz by the FEA. This was only a slight drop but a more attractive design. Similarly, the errors at the nozzle tip as calculated by the error budget spreadsheet were 0.00078, 0.0054, and 0.010 inches for δ_x , δ_y , and δ_z respectively.

With the elimination of the y-axis base feature, the errors at the nozzle tip increased significantly. In an effort to reduce the errors and increase the frequencies at the same time, the size 35 linear guide rail was replaced with a size 55 rail of the same length. The result of the modal analysis was a first natural frequency at 49 Hz, a slight increase compared to the previous structure. The mode shape can be seen in Figure 3.9.

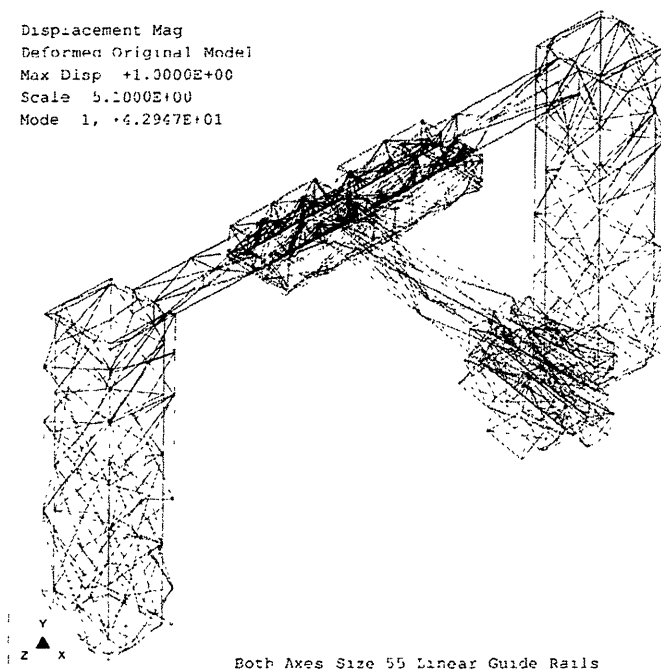


Figure 3.9 FEA Results of Size 55 Rails for Both Axes

Similarly, δ_x , δ_y , and δ_z also improved. They were calculated to be 0.00026, 0.0025, and 0.0058 inches respectively.

The design using size 55 rails for both axes improved on the previous design, and the results show that a bare-rails design is feasible with the shortened y-axis dimensions.

3.2.2 Second Pass FEA Analysis

Once the bare-rails concept was proven analytically, size 55 rails of the required lengths were ordered to build and test a bench-level prototype. At the same time, the bench-level prototype was modeled on Pro/ENGINEER so that FEA analysis could be done in parallel in order to have predicted values as well as compare the validity of the FEA analyses. Figure 3.10 is the solid model of the bench level prototype.

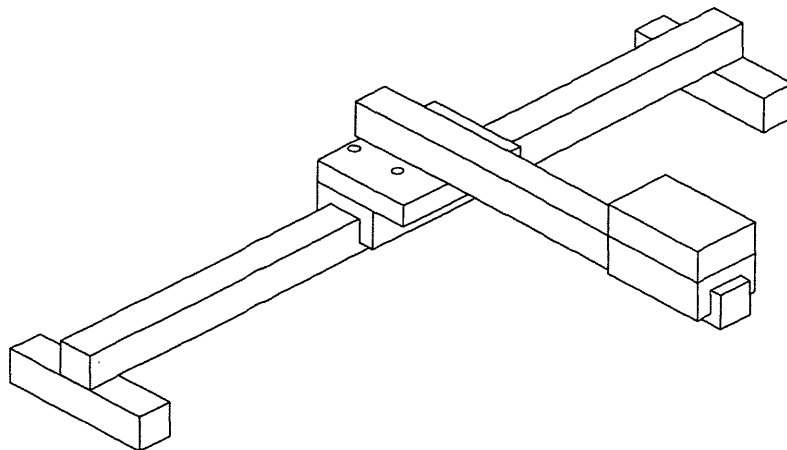


Figure 3.10 Solid Model of Bench-Level Prototype

In this model, the rails and trucks are oriented differently than before. This is to facilitate the installation of the ballscrew system. If the trucks run along the top of the rails, i.e., with the rails are facing up, the ballscrew can easily be mounted on the underside of the rails. It is not desirable to mount the ballscrews along the top since they might bind with the bellows and could cause problems. Also, bottom mounting rails are used since the bolt holes are do not extend all the way through the rail and no unnecessary weakening of the

rail occurs. As before, the 5.79 kg (12.75 lb) mass of steel is to simulate the weight of the nozzle and its components.

For this second pass FEA analyses, the trucks were assigned a more precise modulus of elasticity which was calculated instead of approximated. This was done by using the stiffness data of the size 55 ball bearing truck in moment load, which was obtained from the manufacturer, and applying the specified load while modifying the modulus of the truck in the FEA model until the correct deflection was obtained. This method yielded an equivalent bearing modulus of elasticity of 311,000 psi or 2150 N/mm². This value is about 1/3 of the original approximated equivalent modulus. For this reason, the original FEA results were high with respect to the actual values, however, they were still a valid relative comparison.

As in the bench level prototype, the model was constrained along the bottom surfaces of the two attachment "legs" seen in Figure 3.10 The model analysis was run with the new equivalent modulus and the results were a first natural frequency of 36 Hz, and a second at 72 Hz. The shapes of the modes were consistent with the previous trials. Figure 3.11 shows the FEA model and the first mode shape.

In the following chapter, the bench-level prototype is tested and the actual results are compared to the FEA results.

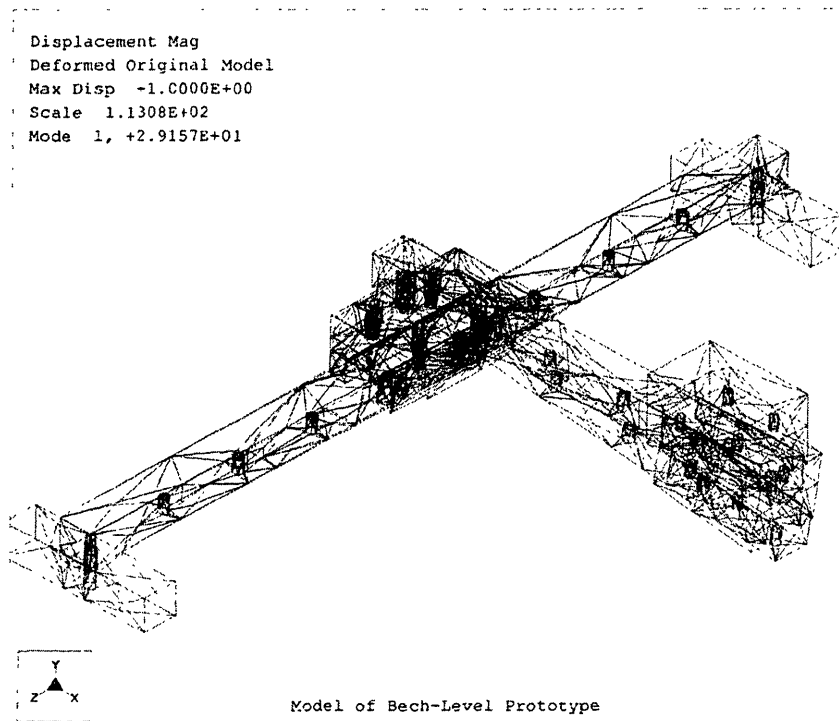


Figure 3.11 FEA Results of the Bench-Level Prototype with One Ball Truck

Chapter 4

STRUCTURAL TESTING

In order to test the validity of the rails-only structure, a series of lab experiments were conducted on the assembled rails. After error analysis and running modal test simulations on Pro/MECHANICA, size 55 rails were selected for the structure as they were predicted to have low enough deflections and high enough natural frequencies. For the single truck tests, a 1 1/4 inch (31.75 mm) thick plate was used to connect the y-axis to the x-axis truck. For the x-axis, a 45-inch (1143-mm) long rail was used while for the y-axis, a 25-inch (635-mm) rail was chosen. These lengths, taking into consideration the space required for the ballscrew system and bellows, will yield an approximate working area of 26 inches by 13 inches (660 mm by 330 mm). This would allow the machining of two 12" x 12" tiles. Long trucks were used on the x-axis while a standard truck was used on the y-axis. The experimental setup was modeled in Pro/ENGINEER and is shown in Figure 4.1 below. The stiffness of the bearings in the FEA model was taken into account by assigning an equivalent Modulus of Elasticity to the truck of 312,000 psi or 2150 N/mm² as explained in Section 3.2.2. The FEA modal simulations on Pro/MECHANICA predicted a first natural frequency at around 29 Hz and a second close to 57 Hz.

The assembled structure was put through a series of experiments to test its behavior in worst-case situations. Two types of medium preload profile rail rolling element bearing systems were tested for the x-axis, those that use ball bearings in the truck as well as those that use cylindrical roller bearings in the truck. All the bolts in the assembly were tight-

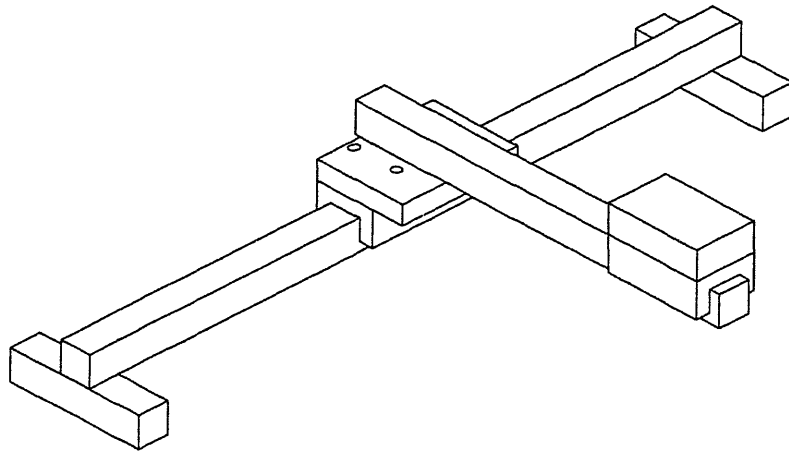


Figure 4.1 Pro/ENGINEER Model of Experimental Setup

ened to 50 foot-pounds using a torque wrench. The assembly was secured to a vary massive granite isolating table using four heavy duty clamps at the ends of the two attachment bars shown in Figure 4.2. Since the worst-case position of the nozzle would be in the mid-

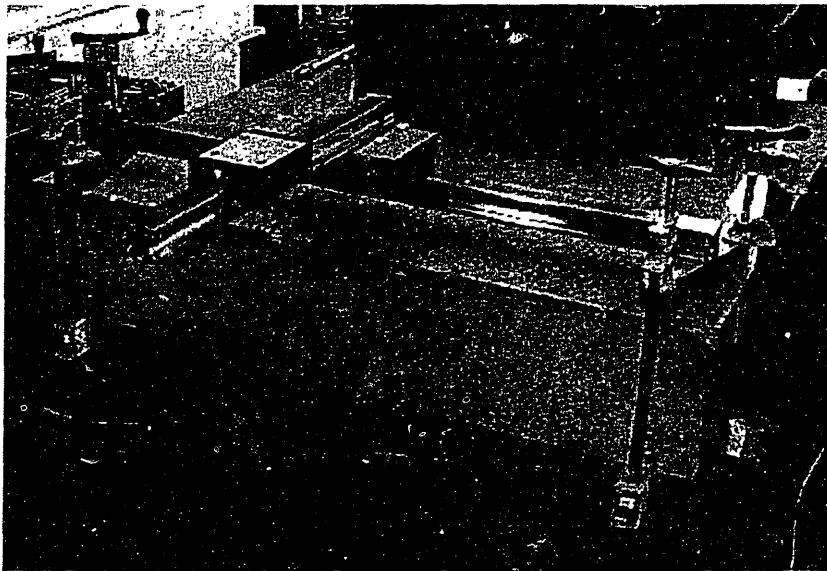


Figure 4.2 The Bench Level Prototype System

dle of the x-axis and the end of the cantilevered member, most of the tests were conducted with the trucks and rails in this position (as shown in Figure 4.1). The rail structure was tested for rail straightness, yaw error at the end of the cantilevered member due to rail errors, static stiffness in the vertical direction at the end of the cantilevered member, and the dynamic stiffness in several different places and configurations on the structure.

4.1 Single Long Ball Bearing Truck

4.1.1 Straightness

Rail straightness was measured in both the horizontal and vertical directions by running a dial indicator along a ceramic beam that is ground flat to within 16 microinches, and taking measurements in 1 inch increments for a 24 inch range of motion. The measurements were taken three times and then averaged. The ceramic beam was placed parallel to the x-axis (the longer rail) and the entire y-axis was moved from left to right with the dial indicator mounted to the bottom end of the shorter rail. The vertical straightness test was done using a 0.0005-inch resolution dial indicator. Since the vertical direction in a waterjet machine is not a sensitive direction, and the range of error was large enough, the 0.0005-inch resolution dial indicator was sufficient. In the horizontal direction, the initial test was also done using the 0.0005-inch resolution indicator. The range of error was considerably smaller, such that the 0.0005-inch resolution of the indicator was not sufficient to show accurate results. Therefore, the test was repeated using a 0.0001-inch resolution indicator. The results of the test can be seen in Figure 4.3.

Vertical straightness ranged approximately 0.00269 inches within the 24-inch range of motion. Again, the vertical direction is not a sensitive direction in a waterjet cutter, so this error will not cause significant problems. The source of this error can be largely attributed to the manufacture of the rails. Since the rails are meant to be bolted down to a base structure, the vertical straightness is not a significant consideration during their manufacture. The fact that for a waterjet cutter, the vertical direction is not a sensitive direction opens up a perfect opportunity for the use of a rail-only structure.

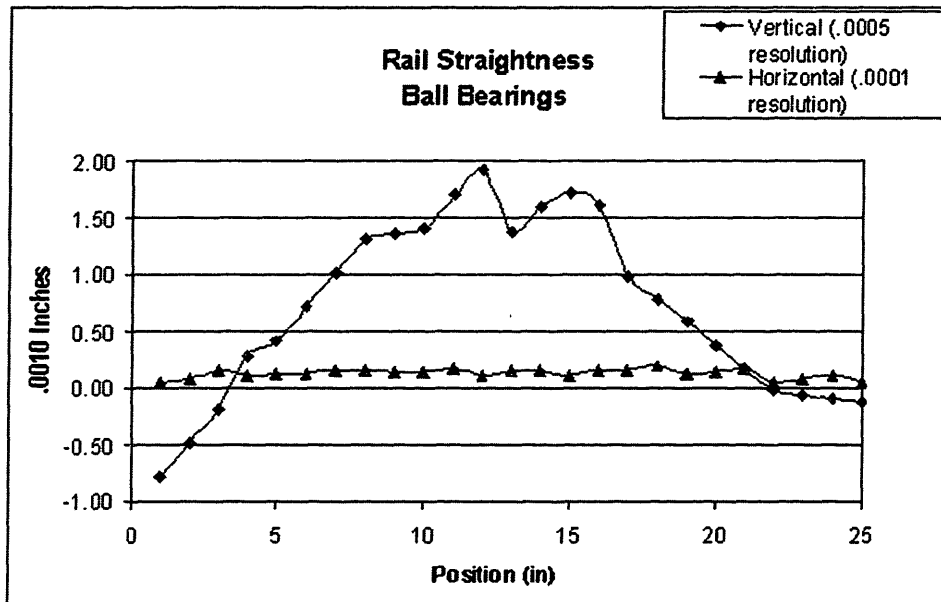


Figure 4.3 Rail Straightness Plot

The horizontal straightness error had a considerably smaller range, 0.00015 inches. The horizontal direction being a sensitive direction, this is a good result. This error is small enough such that this is still a feasible design.

4.1.2 Yaw

Yaw error at the end of the y-axis was measured by using a yaw arm and two 0.0001-inch resolution dial indicators as shown in Figure 4.4.

The distance between the two dial indicators was 14.5 inches and the distance from the middle of the x-axis to the dial indicators was 20.375 inches. The y-axis was moved from the left to the right, taking measurements every 1 inch for a total range of motion of 15 inches. The measurements were taken three times, the difference between each set of measurements calculated, and from that, the relative change in yaw angle calculated. The final three calculated angles for each position measured were then averaged and plotted. Figure 4.5 shows this plot. From this plot, we can see a range of yaw angle error of 23

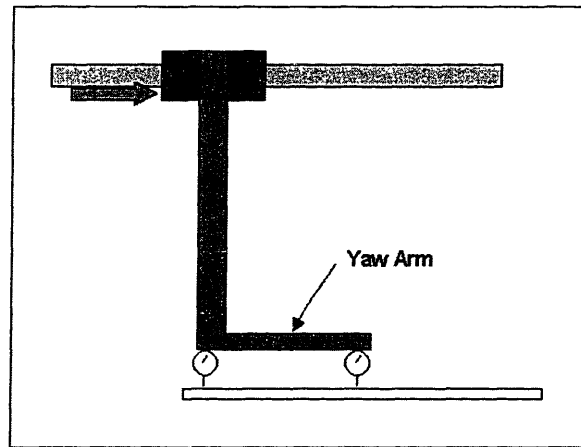


Figure 4.4 Schematic of Yaw Test Setup

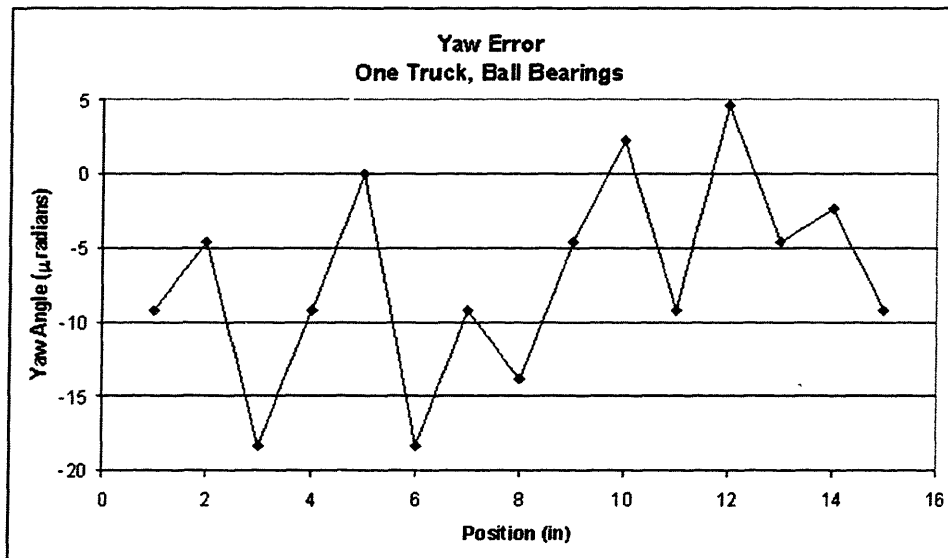


Figure 4.5 Yaw Error, Long Ball Bearing Truck

micro-radians or 0.00132 degrees. This angle results in an x-direction Abbe error of 0.00047 inches at the end of the y-axis. This error is important because a ballscrew drive essentially co-linear to the x-axis would not be able to compensate for this error unless a software error map was utilized.

4.1.3 Static Stiffness

Static stiffness at the end of the cantilevered y-axis was measured by adding weights to the end of the beam and measuring the deflection using the 0.0005-inch resolution dial indicator. The weights used were steel plates weighing 19.5 pounds each. The measurements were started from 0 with no weights, and 4 plates were added with deflection measurements taken after each one. Stiffness measurements were taken with the y-axis positioned on in the middle of the x-axis, 5 inches from the middle, and 10 inches from the middle. The stiffness was calculated for each measurement and then averaged for each position. In the middle location (worst case), the average stiffness was 2745 lb/in (480 N/mm). Five inches from the middle, the average stiffness was calculated as 2926 lb/in (512 N/mm), and at 10 inches from center, 3526 lb/in (617 N/mm). These results are summarized in Figure 4.6. The stiffness of the structure increases as you move away from the center, as is expected. The chart also shows the FEA predicted stiffnesses at the same locations.

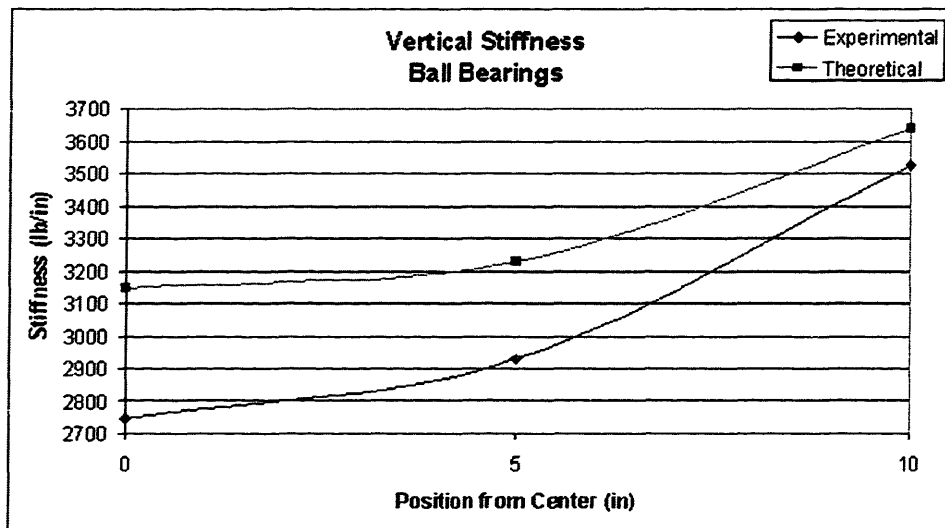


Figure 4.6 Static Vertical Stiffness at End of Cantilever

The FEA results were off by 15%, 10% and 3% compared to the actual results as you go from center, to 5 inches off center, to 10 inches off center.

4.1.4 Dynamic Stiffness

Vibration analysis was also conducted on the rails-only structure. This analysis was done using an accelerometer and a small hammer with an embedded force gage connected to a signal analyzer. The accelerometer was placed in the areas where the vibrations were to be measured. Then, the structure was lightly tapped with the hammer and the signal analyzer would record the vibrations. Each individual configuration measurement was taken 10 times and then averaged by the signal analyzer to yield the plotted data. The damping coefficient, Zeta, was also calculated by the signal analyzer for the desired peaks. Measurements were taken in several places and several configurations and directions in order to get a good understanding of the structure's modal behavior.

As before, the worst case behavior is observed when the y-axis is placed half way on the x-axis and the y-axis truck is placed at the end of the cantilevered rail. Vertical measurements in this configuration were taken first with just the truck, and then with a 12.75-lb (5.790 kg) plate attached to the truck to simulate the weight of the nozzle and support structure. Figure 4.7 shows the modal plot of the structure with just the truck. The first natural frequency is at 36 Hz and the second at 75 Hz. The FEA predicted first mode for the same configuration is around 37 Hz and the second at around 72 Hz. This results in a 3% and a 4% error respectively between the FEA predicted and the measured. The damping coefficient, ζ , for the first peak is 0.001, corresponding to a quality factor Q of 500 according to equation 4.1, which refers to the amplification at the resonance frequency. This high value of Q signifies a poorly damped structure.

$$Q = \frac{1}{2\zeta} \quad (4.1)$$

Once the 12.75-lb (5.790 kg) plate is bolted to the end truck, the first mode frequency decreases, as seen in Figure 4.8. The first mode drops to 28 Hz with the second at 65 Hz.

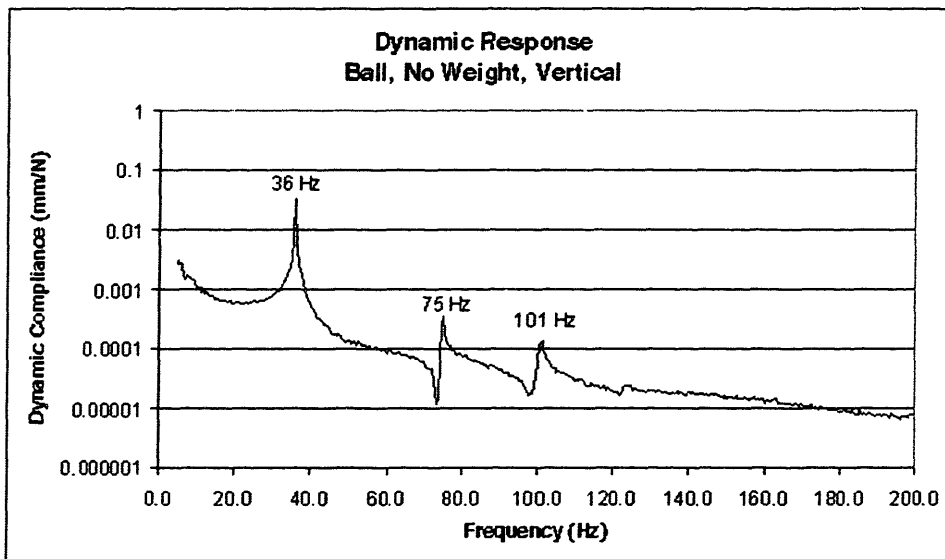


Figure 4.7 Frequency Response, Vertical, No Weight

The predicted frequencies with the weight attached were 29 Hz and 57 Hz, resulting in a 3% and a 12% error respectively between the predicted and the measured. The damping coefficient for the first peak is 0.002, slightly higher than that without the added weight. This corresponds to a Quality factor of 20, still very high. The first frequency is on the borderline of what is desired as the lowest natural frequency. Again, the vertical direction is not sensitive direction, so although important, the side to side mode frequencies are more important.

Side to side modes were excited and measured as well. Figure 4.9 and Figure 4.10 show these measurements with and without the 12.75-lb (5.790 kg) weight. Figure 4.9 shows the mode plot for structure without the weight. The first mode appears at 42 Hz and the second at 96.5 Hz, with a ζ on the first peak of 0.054, considerably higher than for the vertical measurements. The corresponding Q factor is close to 10, an acceptable level of damping.

Figure 4.10 shows the mode plot for Horizontal vibration with the 12.75-lb (5.790 kg) plate bolted onto the truck. The first mode appears at 36.5 Hz. The second mode is at 88

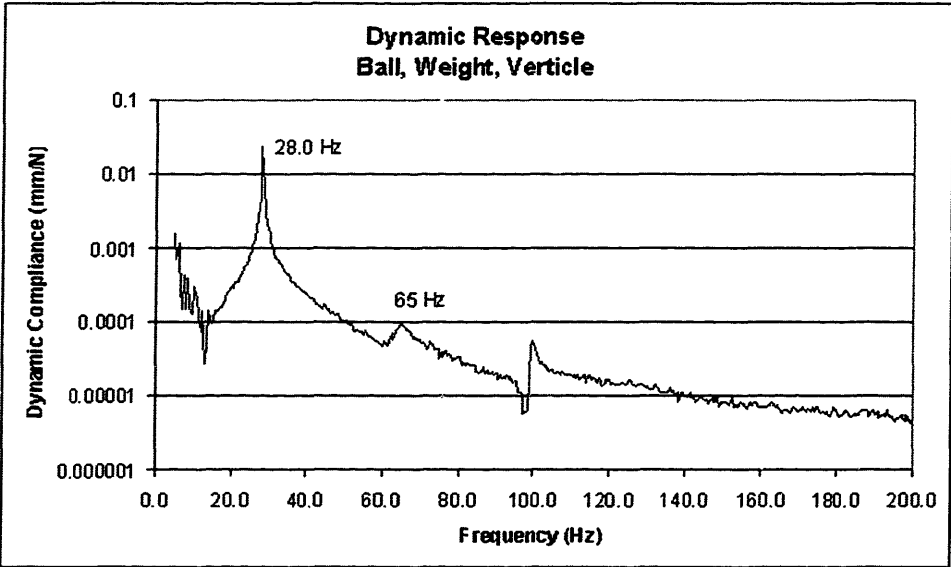


Figure 4.8 Frequency Response, Vertical, With Weight

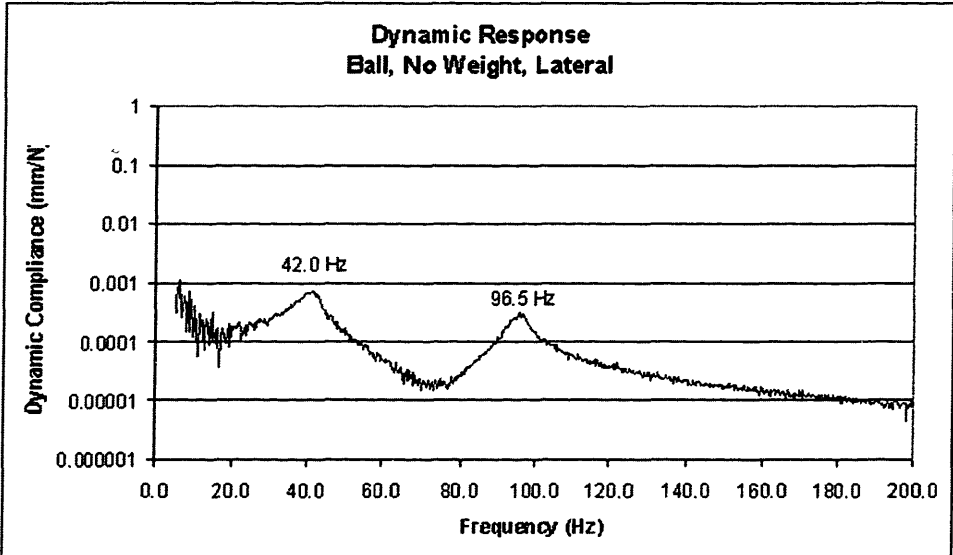


Figure 4.9 Frequency Response, Lateral, No Weight

Hz. The first mode is above the 30 Hz threshold, so it appears at an acceptable level. Additionally, ζ for this peak is 0.046, Q is close to 10, increasing the feasibility of this structural design.

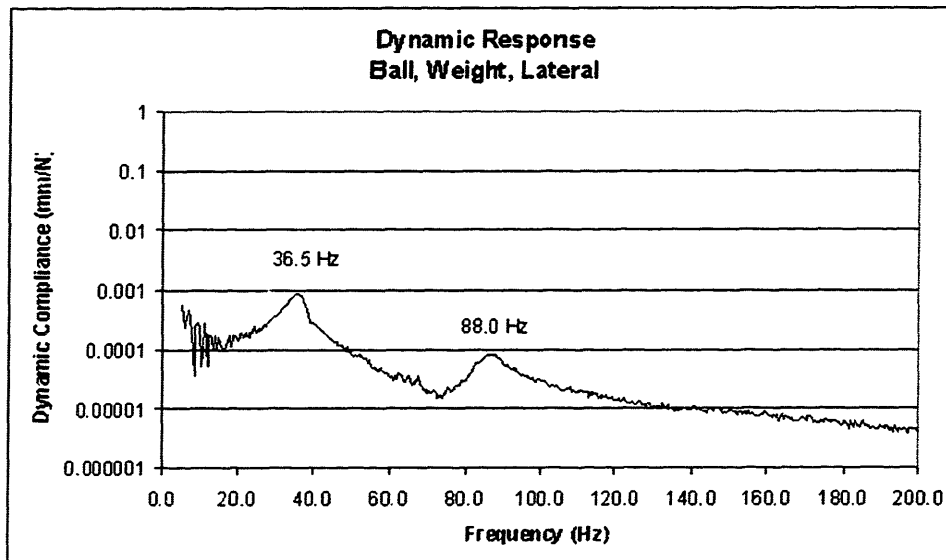


Figure 4.10 Frequency Response, Lateral, With Weight

4.2 Single Long Cylindrical Roller Bearing Truck

As stated before, the same set of tests were run on the same overall structure but using truck with cylindrical roller bearings, also with medium preload, as opposed to ball bearings, and the corresponding x-axis rail. The original ball bearing rail system was used for the y-axis.

4.2.1 Straightness

Straightness was measured for a motion range of 24 inches centered around the middle of the x-axis. Vertical straightness measurements yielded a range of .00234 inches within the 24-inch range of motion. This error is significant, but since the vertical direction is not a

sensitive direction, this error is acceptable. Figure 4.11 is a plot of the rail straightness both horizontally and vertically.

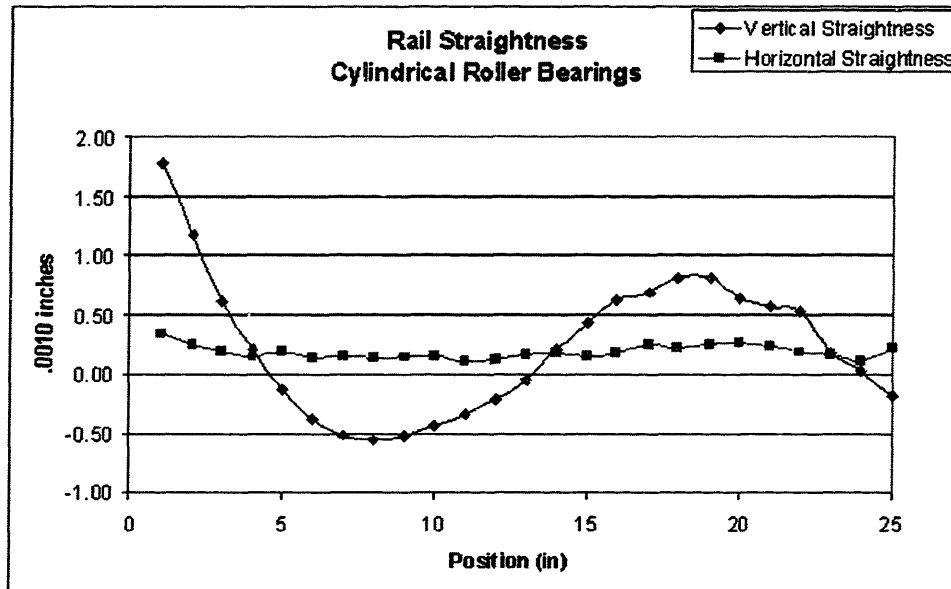


Figure 4.11 Rail Straightness, Cylindrical Roller Bearings

Horizontal straightness measurements yielded a range of .00023 inches within the 24-inch range of motion. Though slightly larger range than for the ball bearing system, this error is not significant enough to render the use of cylindrical roller bearings unusable. In addition, this error can be improved by a more careful selection of the rails. Figure 4.11 shows the results of the measurements.

4.2.2 Yaw

As with the ball bearings, the distance between the dial indicators was 14.5 inches. In this case, however, the distance from the dial indicators to the x-axis was 20 inches. The measured yaw error had a range of 21 micro-radians or 0.00119 degrees. This results in an x-direction Abbe error of 0.00041 inches at the end of the y-axis. As expected, this Abbe error is slightly smaller than that for the ball bearings truck and rail, a 12% improvement.

In both cases, this error cannot be corrected by the x-axis actuator, but it is small enough for the machine to be used as a waterjet cutter. Figure 4.12 shows the plot of the measured yaw angle.

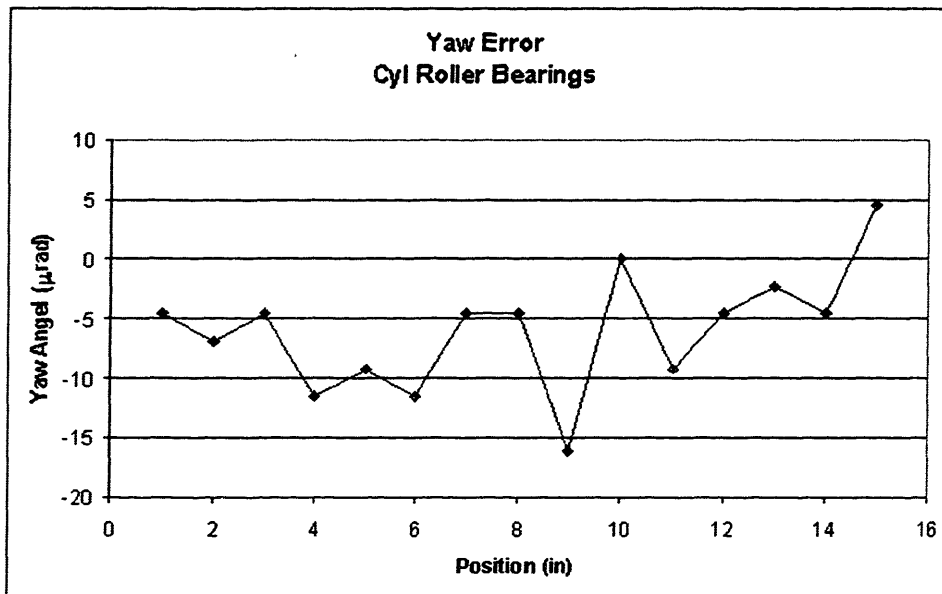


Figure 4.12 Yaw Error, Long Cylindrical Roller Bearing Truck

4.2.3 Static Stiffness

Vertical static stiffness was measured in the same way it was measured for the ball bearing truck and rail system. At the center of the x-axis, the stiffness was measured to be 2447 lb/in (248 N/mm). At 5 and 10 inches from center, the stiffness was 2695 lb/in (472 N/mm) and 3093 lb/in (541 N/mm) respectively. Figure 4.13 shows the measured data. Contrary to expectations, the ball bearing system is 12% stiffer than the cylindrical roller bearing system. This result indicates that the compliance in the system is not due to Hertzian deformation of the balls in the truck but to deformation in the steel of the truck and rails themselves.

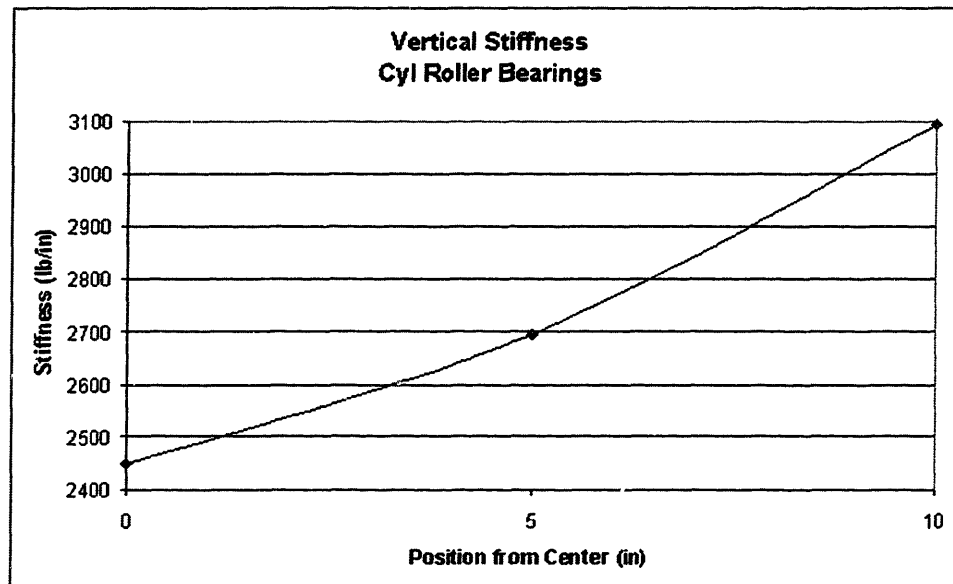


Figure 4.13 Static Stiffness, Cylindrical Roller Bearings

4.2.4 Dynamic Stiffness

Modal analysis was also done on the structure with cylindrical roller bearing system. With the 12.75-lb (5.790 kg) plate bolted onto the truck, vertical modal measurements yielded a first mode peak at 26.8 Hz with $\zeta = 0.002$, and $Q = 250$. A very damped, very small second resonance appears at 67 Hz, it virtually disappears in comparison to the ball bearing system. A significant third peak appears at 102 Hz. Figure 4.14 shows this frequency response. Surprisingly, the first natural frequency when using the cylindrical roller bearings is slightly lower than that for the ball bearings. The difference is only about one 1 Hz, so for comparison purposes, it is practically the same.

Side to side modes appear at 49.8 Hz with a damping coefficient of 0.046 and a quality factor around 10. Figure 4.15 shows this response. In this case, the cylindrical roller bearings do make a significant difference. The first mode increased by 36% from 36.5 Hz to 49.8 Hz. This large difference indicates that the single cylindrical roller bearing truck would be a better choice than the single ball bearing truck for this system.

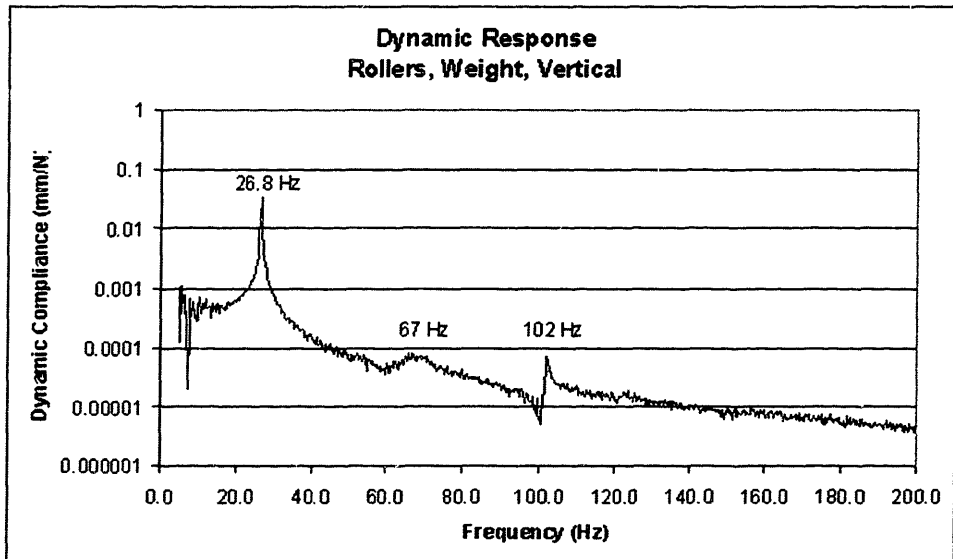


Figure 4.14 Frequency Response, Vertical, Weight

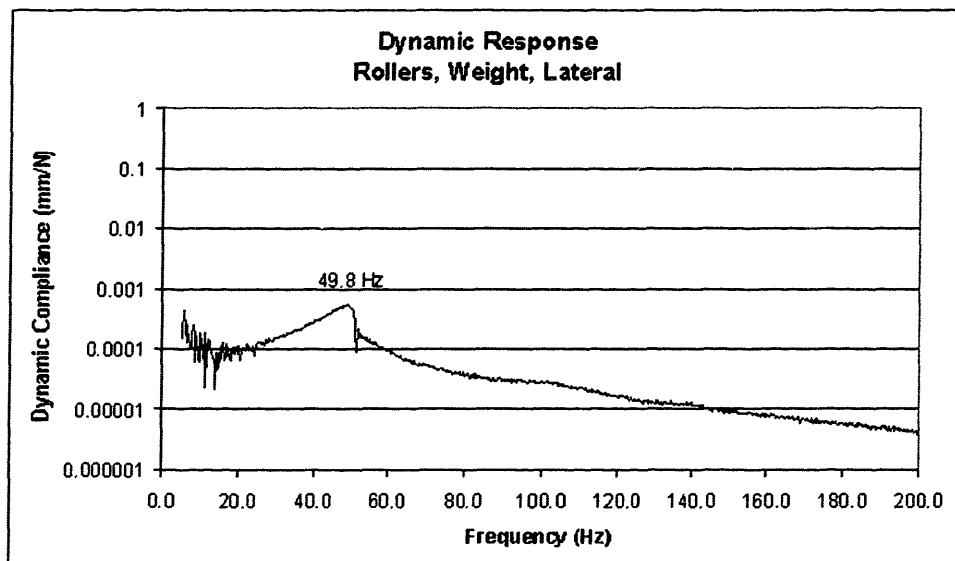


Figure 4.15 Frequency Response, Lateral, Weight

4.3 Two Standard Ball Bearing Trucks

The stiffness tests was also run using two standard ball bearing trucks side by side on the x-axis instead of a single long truck. The tested structure used a 1 inch (25.4 mm) thick plate connecting the y-axis to the two x-axis trucks.

4.3.1 Static Stiffness

As expected, the vertical static stiffness goes up with the addition of an extra truck. With the y-axis placed in the center of the x-axis, the stiffness is 3210 lb/in (561 N/mm). Similarly, 5 and 10 inches from center position, the stiffnesses are 3497 lb/in (612 N/mm) and 4381 lb/in (767 N/mm) respectively. Figure 4.16 shows this stiffness data.

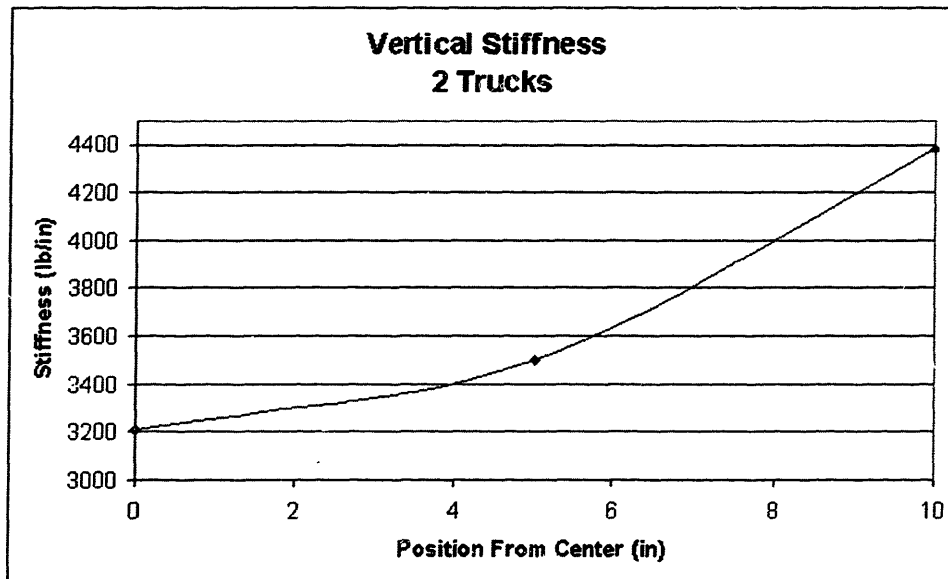


Figure 4.16 Static Stiffness, 2 Standard Ball Bearing Trucks

This stiffness represents almost a 17% improvement over the single ball bearing truck and 31% improvement over the single cylindrical roller bearing truck. These results advocate the use of two standard trucks as opposed to one long one.

4.3.2 Dynamic Stiffness

Vertical modes appeared at 36 Hz and 82 Hz. The first peak had a damping coefficient of 0.003, corresponding to a Q around 165. There is almost a 30% increase in the frequency of the first mode with the introduction of the second truck. Likewise, there is a corresponding increase in the damping of that frequency as well, as is expected. Figure 4.17 shows this result.

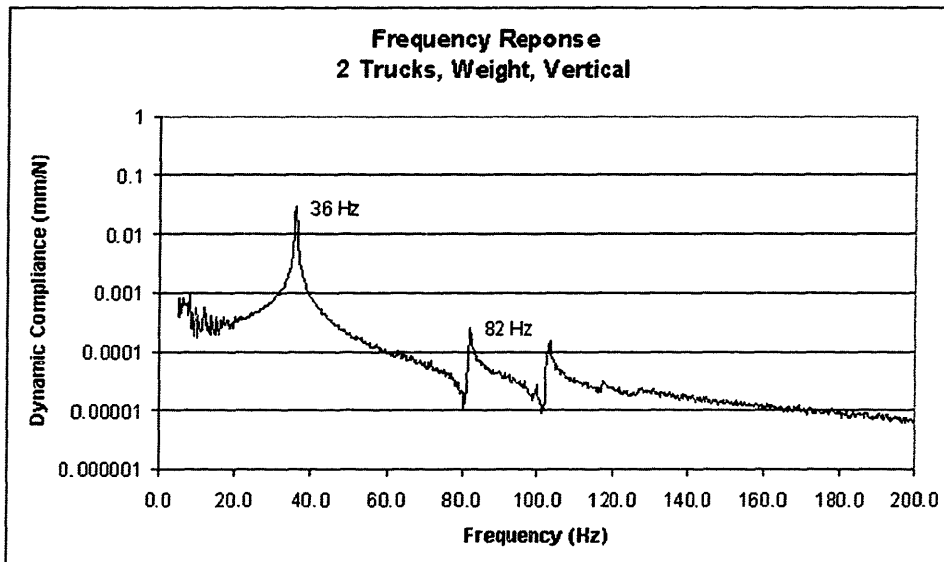


Figure 4.17 Frequency Response, 2 Trucks, Vertical, Weight

Horizontally, the results place the two trucks very close to the single roller bearing truck, at least in terms of the first mode. The first natural frequency appears at 50 Hz and the second at 101 Hz. Figure 4.18 shows this frequency response. There is not a significant increase in the frequency of the first mode with respect to the single roller bearing truck, however the damping is more than doubled, from $\zeta = 0.047$ to $\zeta = 0.103$ and $Q = 5$, which is very good.

Again, these results advocate the use of two standard ball bearing trucks as opposed to a single long truck, ball or cylindrical bearings.

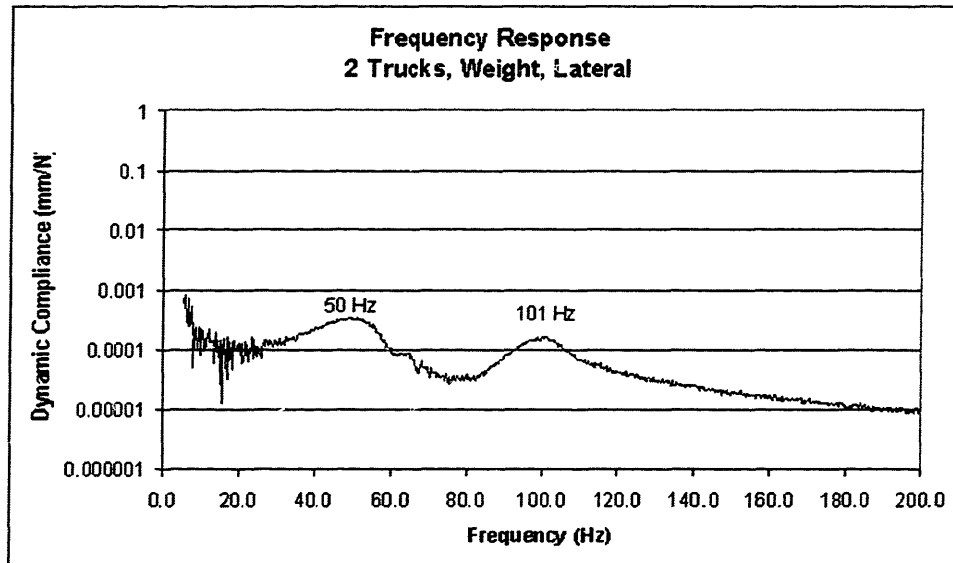


Figure 4.18 Frequency Response, 2 Trucks, Lateral, Weight

4.4 Stiffener and Damper Testing

Once the frequency response behavior of the structure with different truck configurations was known, several different stiffeners and dampers were tested to come up with the best possible arrangement of truck and stiffener/damper combinations. The goal was to raise the first natural frequency observed in the vertical direction and to dampen that frequency response to a more acceptable level. A longer y-axis rail was also tested in combination with a stiffener to see if it was feasible to make the y travel longer than 13 inches.

4.4.1 Stiffeners

Several different stiffeners and attachment locations were tested with the intention of raising the natural frequencies of the structure. The first attempt to stiffen was to bolt a short section of steel C-channel to the bottom of the first quarter segment of the cantilever beam. The actual length of the section was increased to 12 inches (304.8 mm) so that it could be attached by two bolts to the bottom of the rail. The dimensions of the C-channel were calculated such that they would allow the maximum amount of material for stiffen-

ing, but not obstruct the attachment of the ballscrew assemblies or grow the diameter of the bellows to cover the axis. These dimensions for the selected C-channel were 4 inches (101.6 mm) wide by 1.5 inches (38.1 mm) high. The thickness of the channel in the center was 3/16 inches (4.76 mm) but was wider on the sides.

The stiffener was bolted to the structure and vibration analysis was repeated. The first natural frequency in the vertical direction was raised only a fraction of a Hertz, from 28 to 28.3 Hz. This result, along with FEA analyses showing strain energy, indicate that most of the motion in the structure occurs as torsion along the back rail that makes up the x-axis. Therefore, the test was repeated with a similar but longer piece of C-channel bolted to the x-axis rail.

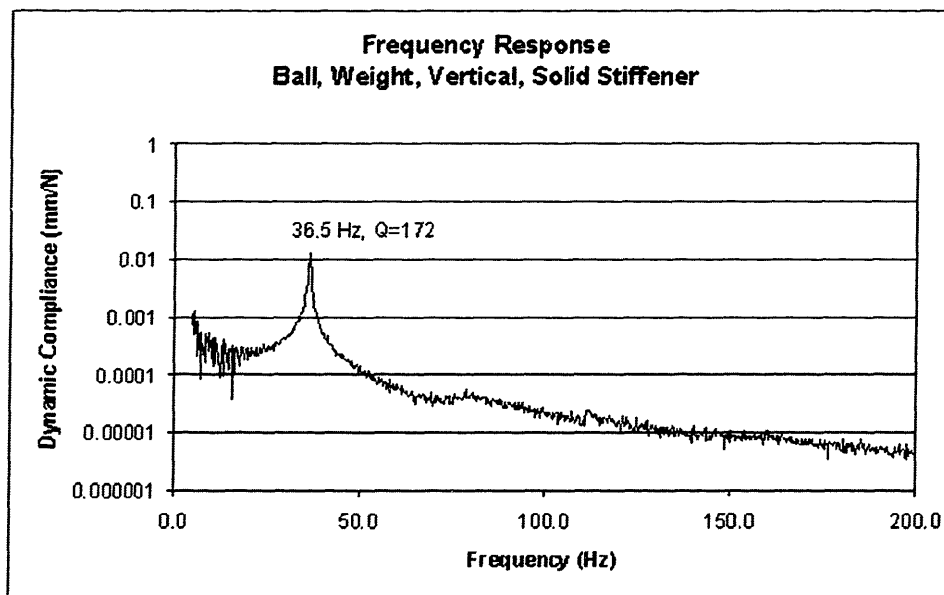


Figure 4.19 Frequency Response with Solid Stiffener Along X-axis

A 35-inch (304.8 mm) length of the same C-channel was bolted along the x-axis and the vibration test was repeated. In this case, the frequency increased by one Hertz. This result is not very good, however it is expected, since the torsional stiffness of C-channel is not

very high. Therefore, in order to more efficiently stiffen the x-axis, which is in torsion, a solid member is required. Attachment of the ballscrew assembly is more flexible on the x-axis, so this solid stiffener does not present a significant problem. The length of C-channel was replaced with a solid length of steel flat ground stock 3 inches (76.2 mm) wide by 1 inch (25.4 mm) high. This time, the frequency was increased significantly from 28 Hz to 36.5 Hz, an increase of 30 %. Figure 4.19 is the frequency response plot of the structure with the solid stiffener attached.

4.4.2 Damper

Once the frequency of the structure was successfully raised, a shear damping material was added between the x-axis rail and the solid stiffener in an effort to dampen the natural frequency response. The damping layer used was a 1/32-inch (0.8 mm) thick layer of "Isodamp" material. Respective vibration tests showed the frequency was lowered 4.5 Hz from 36.5 to 32 Hz and the Q-factor was lowered from 172 to 94. The frequency response

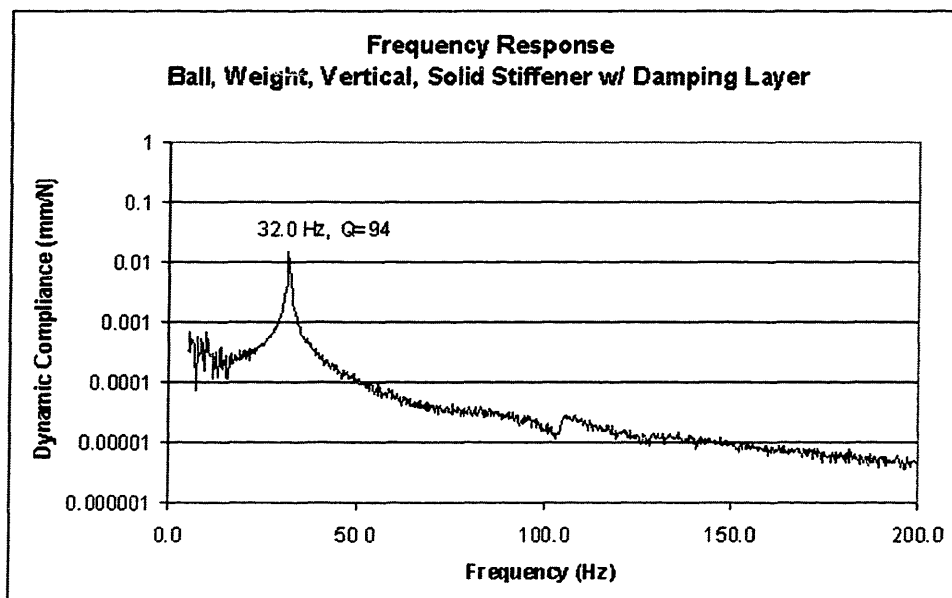


Figure 4.20 Frequency Response with Solid Stiffener and Damping Layer

was effectively dampened, as the Q-factor was reduced by 45%, but the frequency was lowered by 10% at the same time. Figure 4.20 is the frequency response plot of the structure with the stiffener and the damping layer.

4.4.3 Longer Y-axis Rail

In an effort to increase the travel in the y-direction of the final machine and increase the machinable area, a longer y-axis rail was tested using two trucks (standard length with ball bearings) and the solid stiffener. The original 25.5 inch (648 mm) was replaced with a 31-inch (788 mm) rail. The tests for this setup indicated a first natural frequency at 27.5 Hz, which drops below the 30 Hz threshold. The corresponding Q factor is 270, consider-

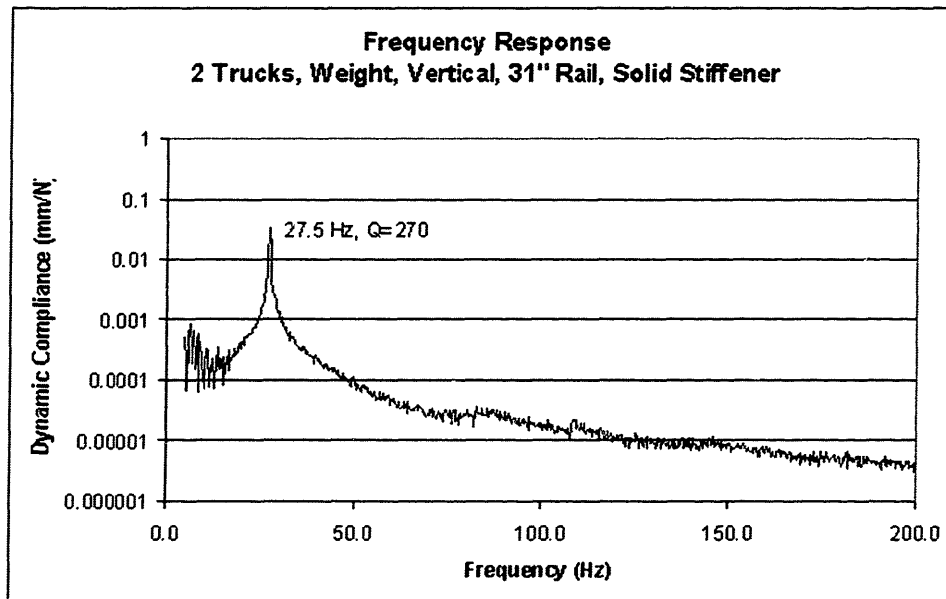


Figure 4.21 Frequency Response for 31" Rail with 2 Trucks and Solid Stiffener

ably worse than the same conditions with the shorter rail. On the other hand, with a damper layer, the frequency is lowered to 25.3 Hz, but the Q factor becomes 122, a con-

siderable improvement. In either case, it seems as if the natural frequency drops too low for this design to be feasible.

4.5 Summary and Conclusion

All the experiments conducted prove that the use of the naked rails structure will work for the construction of a waterjet cutter. Table 4.1 gives a summary of the results of the vibra-

TABLE 4.1 Summary of Frequency Response for all Configurations

Configuration	Travel (in)		1 st ω_n (Hz)	Q-factor	K _{Static} (lb/in)
	X	Y			
One Long Ball Bearing Truck	28	13	28	250	2745
One Long Cylindrical Bearing Truck	28	13	26.8	250	2447
Two Standard Ball Bearing Trucks	26	13	36	160	3210
Solid Stiffener, One Long Ball Truck	28	13	36.5	172	3774
Solid Stiffener with Damping Layer, One Long Ball Truck	28	13	32	94	3000
31" y-axis with Solid Stiffener, 2 Standard Ball Trucks	26	18	27.5	270	2839
31" y-axis with Solid Stiffener and Damping Layer, 2 Standard Ball Trucks	26	18	25.3	122	2646

tion experiments in the vertical direction with the weight attached to the truck, which is where most of the borderline behavior is observed. From this condensed table, it is easy to determine that best configuration would be to use two standard trucks with the solid stiffener. This would significantly raise the first natural frequency of the system and would compensate for the inherent lowering of the frequency upon the addition of the posts to the system.

Chapter 5

FINAL DESIGN AND SOLID MODELING

Once the bare-rails concept was proven with the testing of the bench-level prototype, the rest of the abrasive waterjet cutter was designed and modeled on Pro/ENGINEER, starting with the base structure analyzed in Chapter 4. One of the goals of this design was a machine that is inexpensive to manufacture and inexpensive to assemble. For this reason, every effort was taken to minimize the number of precision machined parts, and to use as many off-the-shelf parts as possible. The final section of this chapter shows the bill of materials for the entire machine and the estimated cost of each part.

5.1 Ball Rail and Ballscrew System

As described in previous chapters, size 55 linear guide rails are used as the structure of the machine. The x-axis rail needed to achieve a travel of 660 mm (26 in) by the y-axis is 1250 mm (49.2 in) long. The y-axis rail needed for a travel of 330 mm (13 in) by the nozzle carriage is 770 mm (30.3 in). The two axes are attached to each other by a mountplate that is attached to two standard size 55 steel runner blocks (trucks). The y-axis rail is then attached directly to the 28.5 mm (1.125-inch) mountplate. The mountplate is machined out of 28.575 mm (1 1/8 in) thick flat ground steel stock. In addition, the solid stiffener, also made out of flat ground steel stock, discussed in Chapter 4, is attached to the bottom of the x-axis rail along most of the length. Figure 5.1 clearly shows this assembly.

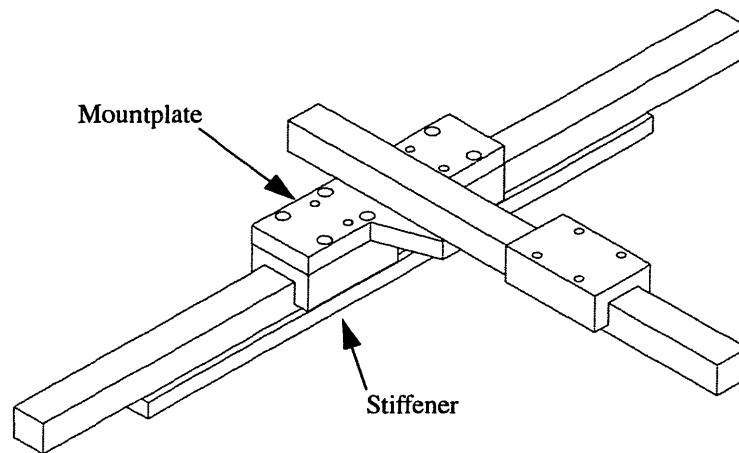


Figure 5.1 Rail Assembly

Taking into account the functional requirements of maximum acceleration, maximum velocities, and the weights being transported, and using a spreadsheet developed in the lab, a 16 mm (0.63 in) ballscrew with a 10 mm (0.4 in) pitch was chosen. The length of the ballscrew required for the x-axis is 1205 mm (47.5 in), and for the y-axis, a 725 mm (28.5 in) ballscrew is required.

The system is designed so that the ballscrews run underneath the rails, and both the rail and the ballscrew are covered by bellows. The ballscrew actuating the y-axis runs beneath

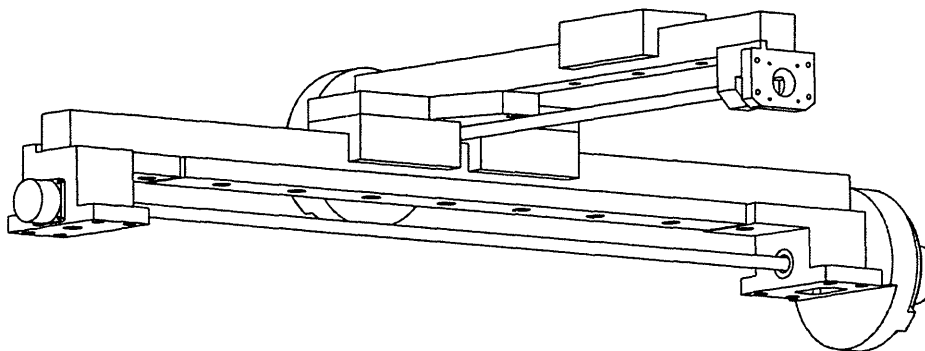


Figure 5.2 Assembly Showing Ballscrew Locations

the mountplate, above the x-axis rail, and between the two trucks to the back of the machine where the motor is mounted, as seen in Figure 5.2. For this reason, careful consideration had to be used in choosing the thicknesses of the y-axis bearing blocks and the mountplate.

5.2 Bearing Blocks

The bearing blocks at the extremes of each axis are the only precision machined parts in the design. In an effort to minimize the number of machined parts needed, the bearing blocks were designed to serve as the pillow blocks for the ballscrew, the attachment adapter for the bellows endplates, the attachment adapter for the motor and encoder, and in the case of the X-axis, the point of attachment to the tank.

In order to minimize cost and weight, the possibility of making the bearing blocks out of aluminum was explored. The y-axis bearing blocks are not subjected to high forces, and the difference in temperature between the aluminum block and the steel ballscrew or bearing will not be significant enough to cause problems due to different thermal expansion coefficients. Furthermore, a well anodized aluminum part will prevent corrosion due to galvanic effects. For these reasons, aluminum bearing blocks for the y-axis will work.

It was not clear, however, whether or not aluminum would work for the x-axis bearing blocks since they are supporting all the loads and moments due to the weight of the machine. To decide this, an FEA analysis was run on the smaller of the two x-axis bearing blocks, the one that mounts the encoder, to see whether it could handle the loads it would be exposed to. Figure 5.3 shows the results of the FEA analysis. The part assembled to the bearing block in the figure was used to apply the loads and moments applied by the weight of the machine. The maximum stress felt by the aluminum bearing block as given by the FEA was close to 20 N/mm^2 , well under the yield strength of aluminum. However, the maximum displacement was 0.06 mm, which occurred at the corner of the flange as seen in the figure. This small deflection yields an abbe error at the nozzle tip in the y direction of 0.5 mm (.020 inches) when the nozzle carriage is at the outermost position.

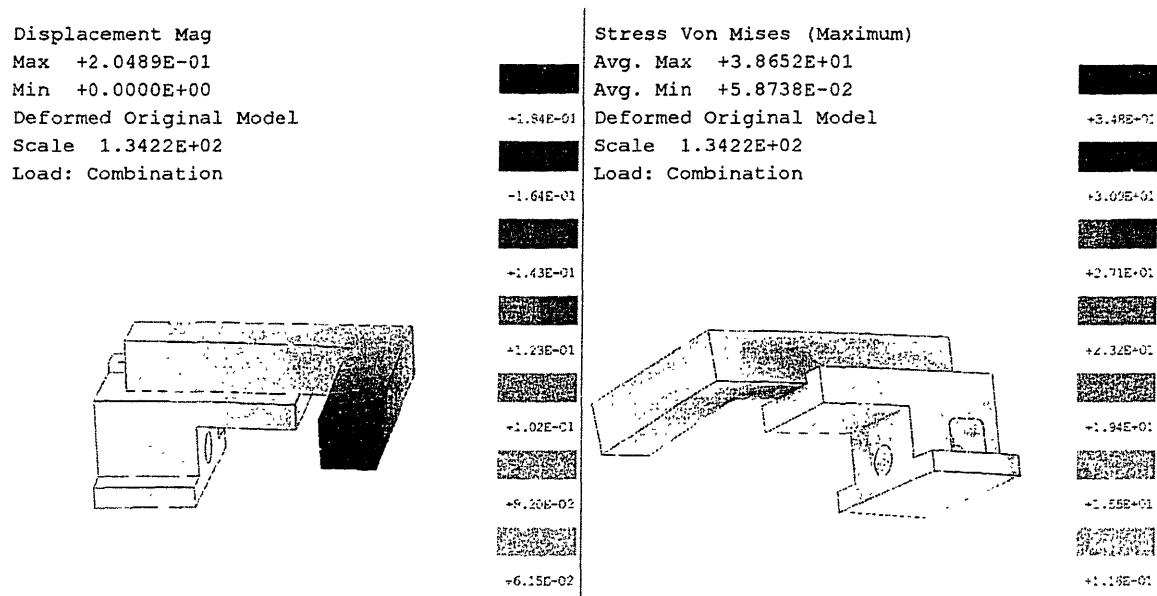


Figure 5.3 FEA Results From Bearing Block Analysis

This changing deflection would significantly impact the accuracy of the machine and therefore is significant enough to justify the use of steel x-axis bearing blocks.

5.2.1 X-Axis Motor Mount Bearing Block

As mentioned above, this bearing block incorporates the mounting of the motor, the ballscrew, the bellows endplate, and attachment to the tank into one part constructed out of steel. This block is pictured in Figure 5.4. Since the machine is designed such that the linear rails are the precision surfaces and structure onto which all other parts are attached, the bearing blocks have precision reference surfaces that mate to those on the rail to ensure proper alignment. The top surface of the bearing block is the mating surface to the bottom of the linear guide rail. It is bolted to the rail using the two mounting holes shown. The raised "lip" is the precision reference surface to be pressed up against the side of the rail (a reference surface) during assembly to ensure that all the components are aligned as intended. Underneath the rail mating surface is located the precision hole for the fixed bearing used by the ballscrew. The motor is attached to the back of the part via a pilot hole and mounting bolt holes. The motor shaft is attached to the ballscrew by a flexible steel

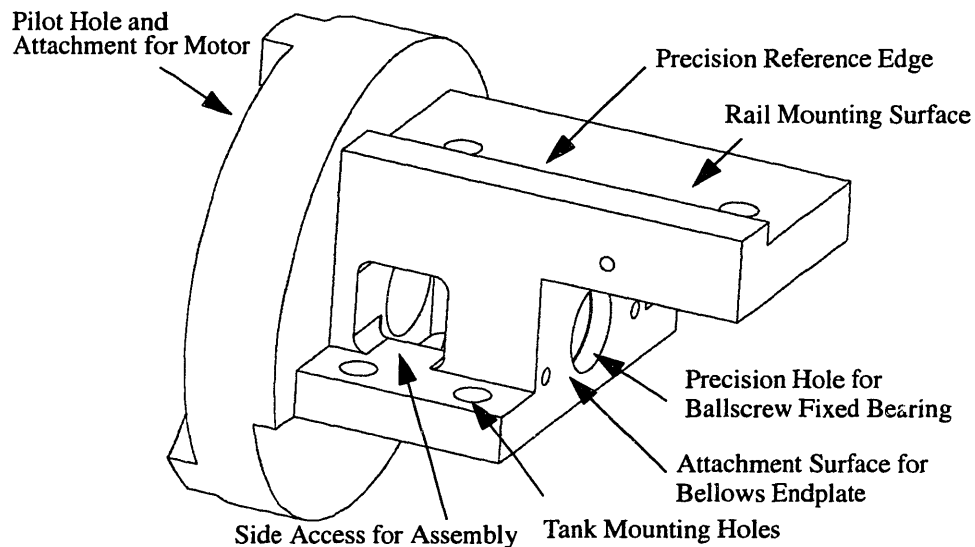


Figure 5.4 X-Axis Motor Mount Bearing Block

bellows coupling with high torque, zero backlash characteristics. Figure 5.5 shows how this section of the assembly goes together.

5.2.2 X-Axis Encoder Mount Bearing Block

This part is the complementary part to the x-axis motor mount bearing block. It is located at the opposite end of the x-axis linear rail and serves as the mounting block for the encoder, the ballscrew floating bearing, and the opposite bellows endplate. As with the previous bearing block, it also attaches the entire assembly to the base feature and is therefore machined out of steel. Shown in Figure 5.6, it has many of the same features as the x-axis motor mount bearing block, but it mounts the encoder as opposed to the motor.

The encoder was mounted on the opposite end of the motor for two main reasons. First, the motor that is being used is an inexpensive motor that does not have the capability to connect to a modular encoder. Second, an encoder attached to the ballscrew opposite the motor yields a more precise reading of the position of the carriage since there is no error introduced by torsion in the ballscrew as a result of the torque applied by the motor. This

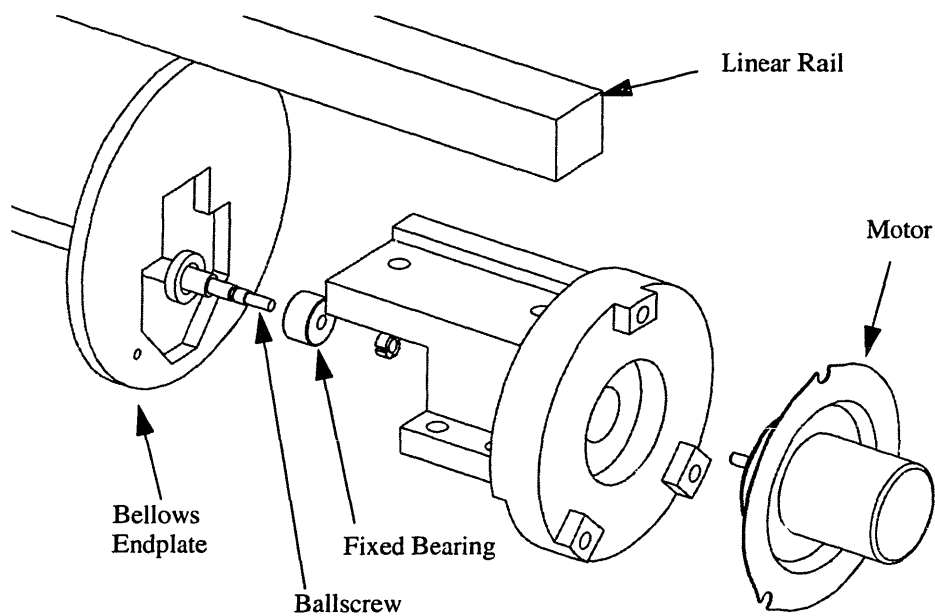


Figure 5.5 Exploded View of X-axis Motor Mount Bearing Block Assembly

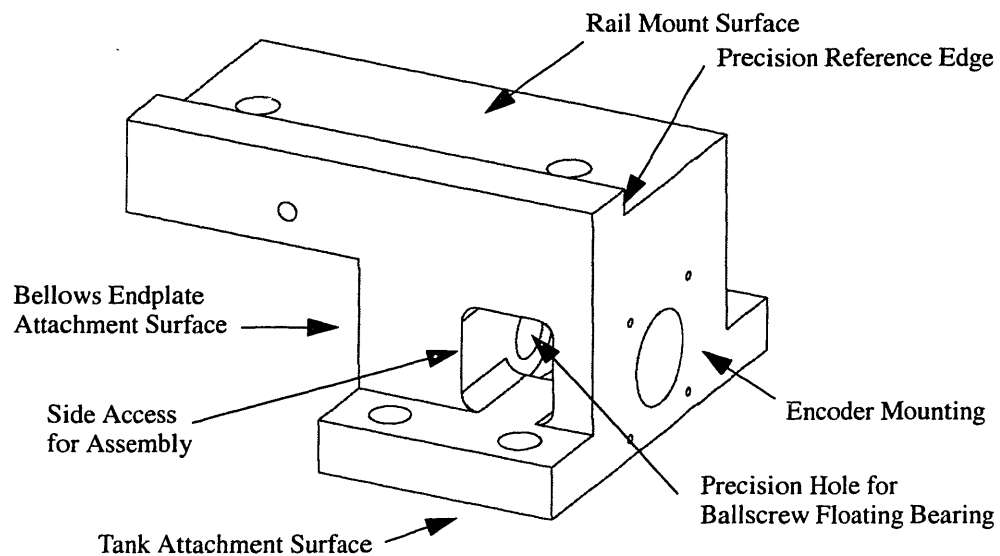


Figure 5.6 Y-Axis Encoder Mount Bearing Block

occurs since beyond the ballnut, the ballscrew is not loaded, therefore there are no angular deflections.

5.2.3 Y-Axis Motor Mount Bearing Block

The y-axis bearing blocks are similar to those for the x-axis, except they only attach to the y-axis rail and are a little smaller. Because they are not under high loads, the y-axis bearing blocks are made out of anodized aluminum to minimize both cost and weight. The y-

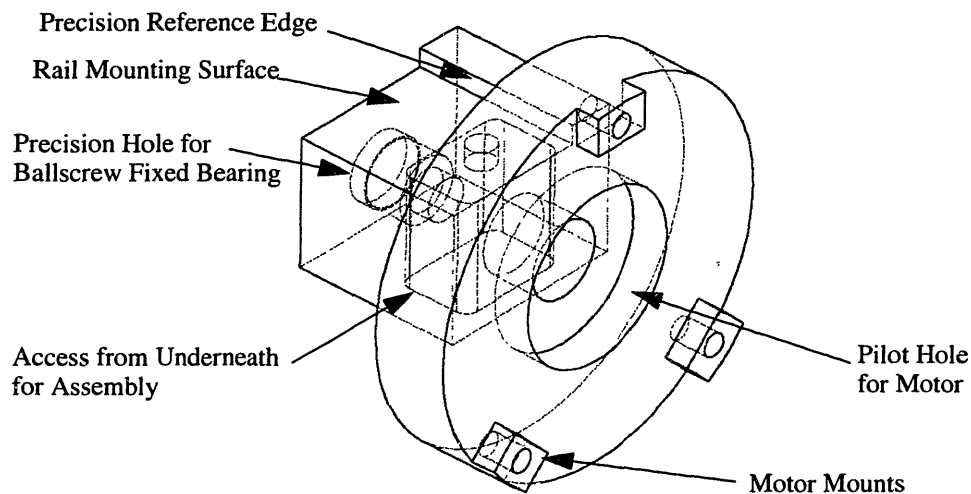


Figure 5.7 Y-Axis Motor Mount Bearing Block

axis motor mount bearing block is shown in Figure 5.7. It attaches to the y-axis linear rail by one bolt as opposed to two and is slightly smaller than its x-axis counterpart. Also, this part does not support a bellows endplate due to its location in the assembly. This is illustrated in later sections.

5.2.4 Y-Axis Encoder Mount Bearing Block

Figure 5.8 shows the encoder mount bearing block that opposes the motor mount bearing block on the y-axis. Again, it is slightly smaller than the x-axis version and attaches to the rail using one bolt. The assembly of this part is shown in the exploded view in Figure 5.9

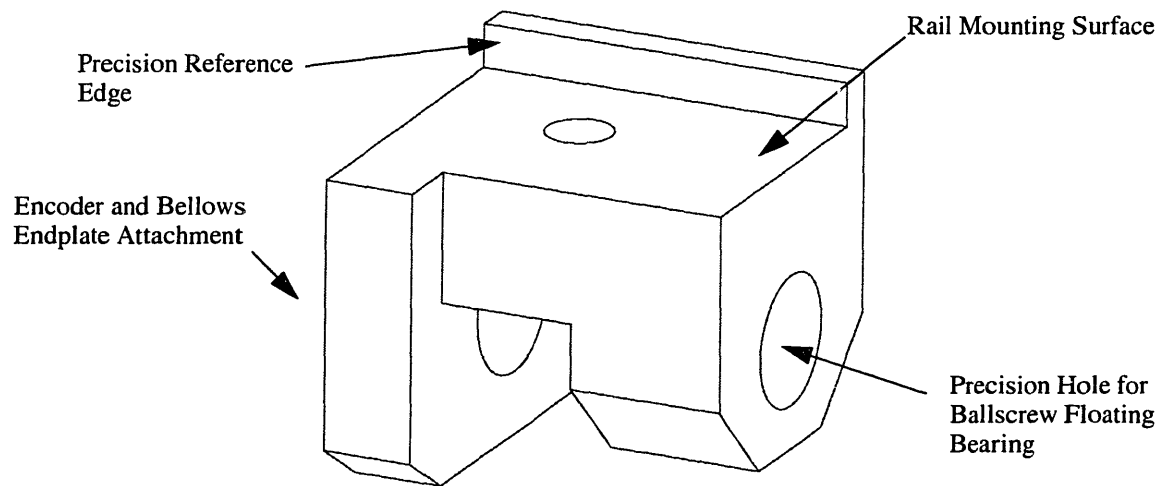


Figure 5.8 Y-Axis Encoder Mount Bearing Block

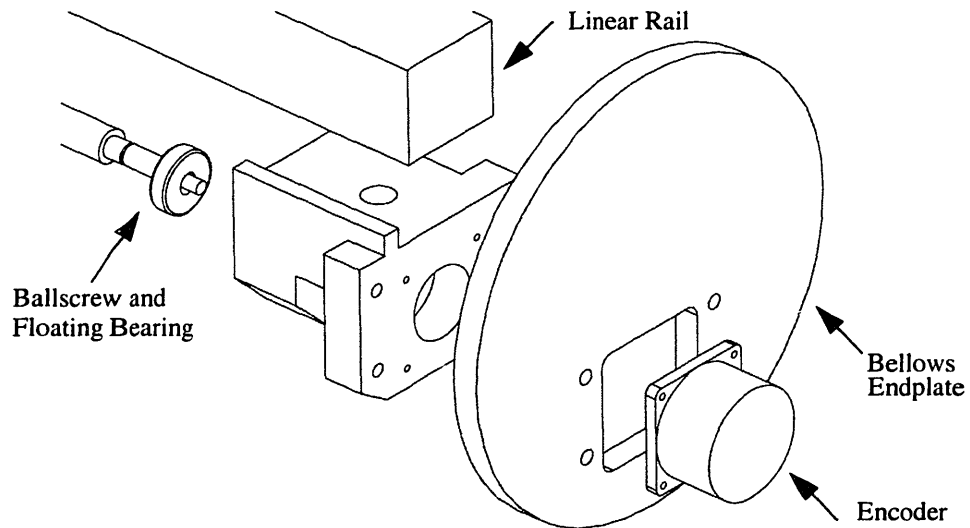


Figure 5.9 Exploded View of Y-Axis Encoder Mount Bearing Block Assembly

5.3 Carriages and Ball Nut Mounting

In keeping with the goal of minimizing the number of precision machined parts required for the system, the ball nuts are mounted such that they can be "floated" to their natural

position, and then the bolts tightened to maintain this position. In order to accomplish this, the nut-mounting plates are designed to attach horizontally to the runner blocks, and vertically to the nut housings. In this way the nut could effectively be floated in both directions during assembly. Enough slop is allowed in the bolt clearance holes for slight yaw and pitch adjustments as well. Figure 5.10 shows the design of the nut-mounting

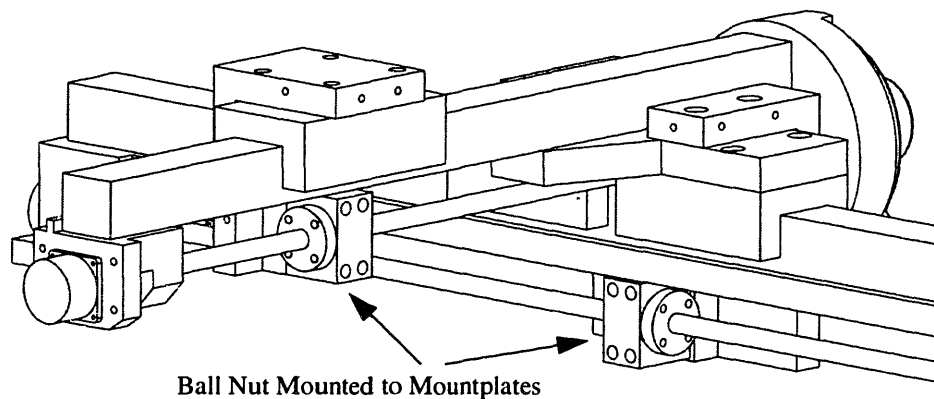


Figure 5.10 Ballscrew Nut Mounting

plates and illustrates the idea of mounting the nut by floating it.

The ball nut mounting plates and their cover plates, discussed in more detail in Section 5.5 are not heavily loaded and are therefore both made out of anodized aluminum to minimize weight and cost.

5.4 Motors and Encoders

The same spreadsheet that was used to calculate the size and pitch of the ballscrew also gave the motor requirements needed to accomplish the functional requirements related to movement. These requirements were a maximum torque of 0.5 N-m and a constant torque of 0.2 N-m at 600 RPM. A high volume motor used in the automotive industry was found that meets these requirements, making it a very inexpensive alternative, around \$30 per

motor, compared to the relatively expensive servo-motors usually employed for these tasks which could cost anywhere from 3 to 10 times as much. As discussed in Section 5.2.2, the use of this motor prompted the assembly of the optical encoder on the opposite side of the ballscrew.

For the selection of the rotary optical encoder, the functional requirements and the selected ballscrew had to be considered. An original functional requirement was the need for a resolution of at least .0005 inches/step, or .0127 mm/step. Since a 10 mm pitch ballscrew was selected, an optical encoder with at least 790 counts per revolution is needed. It was not difficult to find an inexpensive encoder with this count density. In addition, attaching the encoder to the ballscrew using a flexible coupling will eliminate the need for a very precise attachment surface.

5.5 Sealing

Due to the inherently harsh and dirty working environment of an abrasive waterjet cutter, all the bearings and ballscrews need to be sealed to protect them from splashing water and abrasive. This is accomplished with the use of bellows completely surrounding both axes of the machine. For this reason, another initial goal of the design was to minimize the required bellows diameter. With the current design, the smallest bellows that could be achieved had an inner diameter of 190.5 mm (7.5 in) for the x-axis, and 165.1 mm (6.5 in) for the y-axis. In order to achieve a 10:1 expanded to compressed length ratio, a 25.4 mm (1 in) fold is required such that the outer diameter is 50.8 mm (2 in) larger than the inner diameter. The expanded and contracted lengths of the bellows are 736.6 mm (29 in) and 76.2 mm (3 in) respectively for the x-axis pair, and 368 mm (14.5 in) and 38.2 mm (1.4 in) respectively for the y-axis pair. These extended and retraced lengths can be seen in the solid model in Figure 5.11.

Due to the length of the x-axis bellows, an internal guide had to be incorporated into the design to support the bellows. This was done using two 6.35 mm (1/4 in) stainless steel rods running from one end of the x-axis to the other. These rods glide in grooves milled

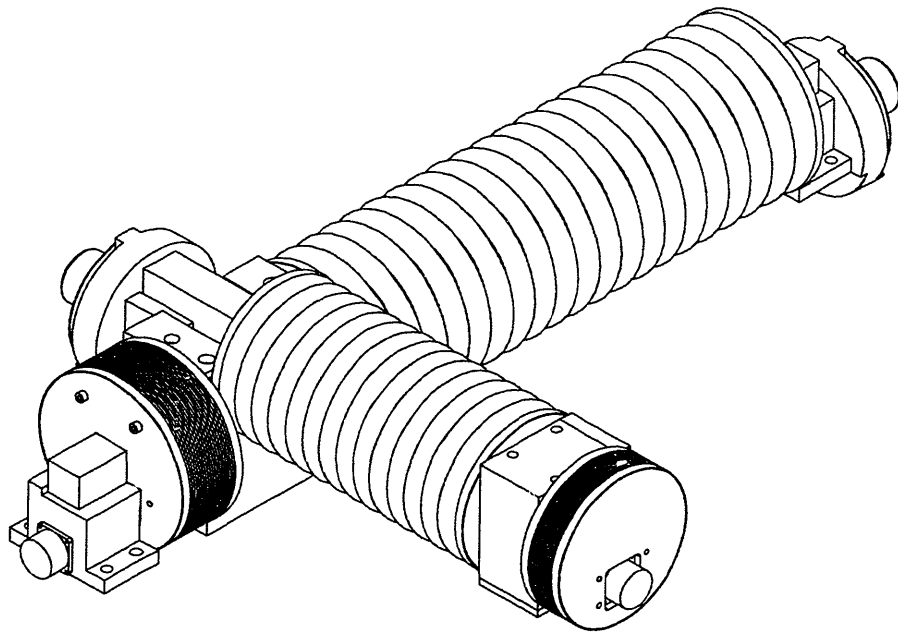


Figure 5.11 Solid Model Showing Maximum and Minimum Bellows Lengths

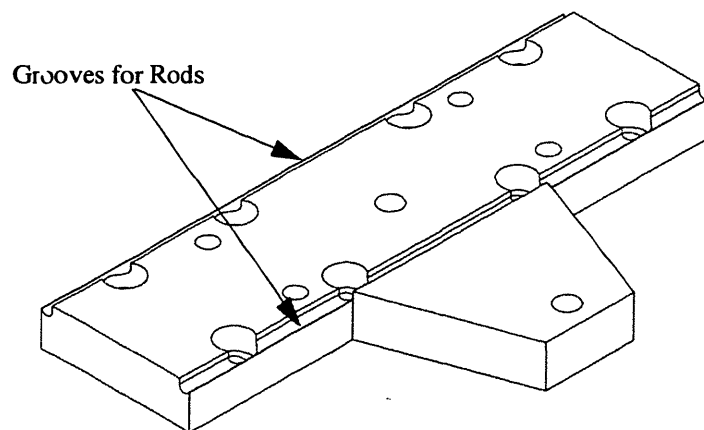


Figure 5.12 Mountplate Showing Grooves for Internal Bellows Guide Rods

into the mountplate that unites the two axes as shown in Figure 5.12. The grooves allow the rods to glide under the parts that are attached to the mountplate, including the y-axis rail. The bellows in turn glide on these rods. Figure 5.13 shows the guide rod configuration.

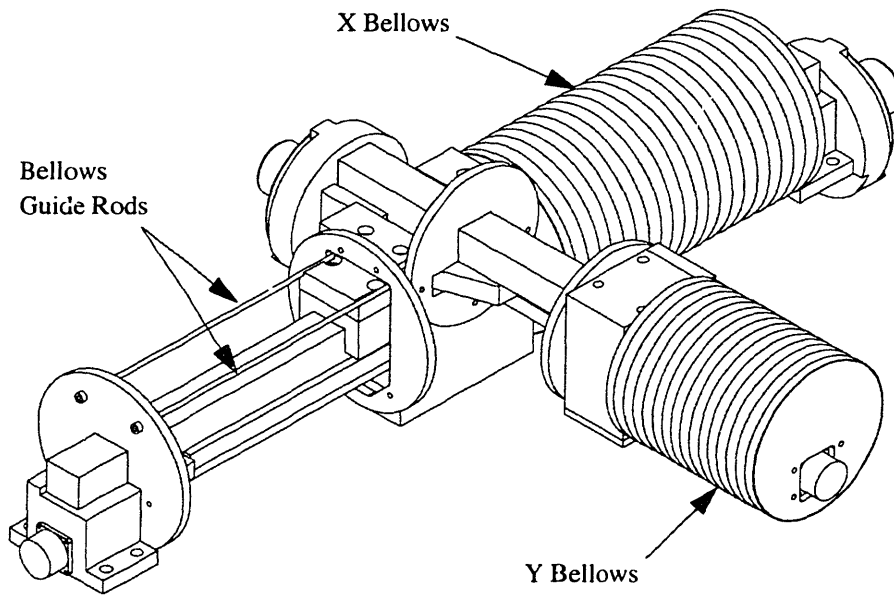


Figure 5.13 Assembly of the Small Waterjet Showing Bellows and Internal Guide Rods

In combination with the bellows, endplates were designed to seal the ends. The bellows are attached to these endplates via a collar molded into the bellows and hose clamps. In the case of the interior endplates, they are attached to the nut-mounting plates and covers creating a seal on either side of the plate. The external endplates, on the other hand, only create a sealed environment towards the bellows side. The endplates are designed out of ABS plastic so that they can easily and inexpensively be cut on a waterjet out of 12.7 mm (1/2 in) thick sheets without any secondary machining.

The components on either side of the interior endplates are sealed by a two part anodized aluminum enclosure mentioned in Section 5.3. One side of this enclosure is made up of

nut-mounting plate, and the other side is a corresponding cover plate. Figure 5.14 shows this arrangement.

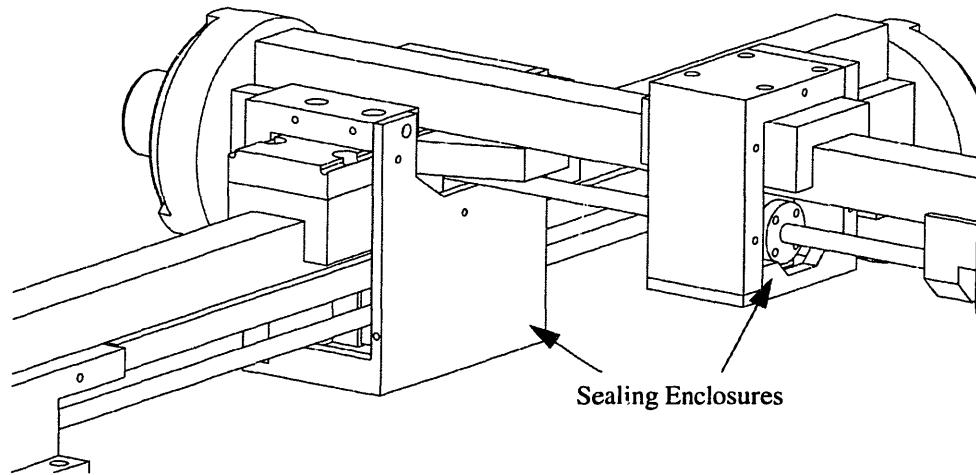


Figure 5.14 Enclosures Sealing Components between Bellows

With the above-discussed set of sealing components, all the vital parts of the machine are sealed and protected from the water and abrasive introduced to the machine during normal use.

5.6 Tank

A waterjet cutter requires a tank filled with water to receive the jet of water and abrasive from the nozzle, but also to drown out the noise and minimize the mess by allowing the actual machining to be done under water. The tank for this machine is designed to be cast out of polymer concrete. The design incorporates the posts that support the structure into the tank and allows the rest of the assembly to be bolted directly onto those posts. The tank is to be cast using a two part mold with a parting line at the rim of the tank. A draft angle of 3 degrees is used for all sides of the tank except the front, on which a 10 degree draft is used. This increased draft is to create space underneath the front edge of the tank

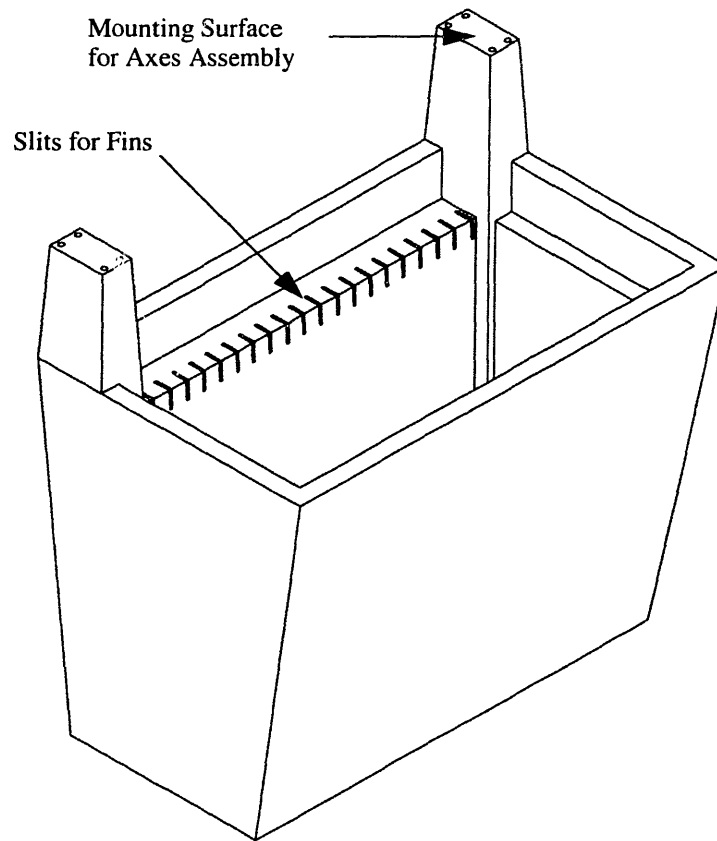


Figure 5.15 Polymer Concrete Tank

for the operators' feet so that the machine is more comfortable and ergonomic to use. The rim of the tank is 1016 mm (40 in) high and the posts are 303 mm (11.9 in) tall, which puts the central axis of the y-arm 457 mm (18 in) above the rim of the tank. Figure 5.15 shows the design of the tank.

In order to support the workpiece, a number of hot-dipped galvanized steel fins are used. These fins need to be replaceable since they are damaged as the waterjet slowly cuts into them while machining parts. The slots for these fins were designed into the mold of the tank such that no additional parts are required to hold the fins in place. The fins are placed in the slots and can be turned over or replaced as needed.

5.7 Bill of Materials and Cost

Table 5.1 lists all the components that comprise the small waterjet machine, the quantity of each part needed, and their estimated cost (quoted for a quantity of 100). From this list, including estimated assembly costs, the cost of the machine is calculated.

The small waterjet cutter is made up of 38 different parts. About half the parts are off-the-shelf parts and half machined parts. Of the machine parts, however, only four, the bearing blocks, need to be precision machined and include any level of complexity. The other machined parts are relatively simple in design.

The assembly of the machine was estimated to take an average of 10 hours over 100 machines at \$20/hr. The quoted costs of 38 parts in addition to the estimated assembly cost bring the total estimated cost of the machine to \$9,048.15. The calculated cost is estimated to be within 10% of the actual cost, allowing for any error in estimation.

TABLE 5.1 Bill of Materials and Cost of Machine

Qty	Description	Piece Price*	Tot Price
Off-the-Shelf Parts			
1	size 55 rail, 1250 mm long	\$412.11	\$412.11
1	size 55 rail, 770 mm long	\$260.63	\$260.63
3	size 55 slimline standard truck	\$170.61	\$511.83
1	16 mm ballscrew L=1205, L1=1105	\$490.00	\$490.00
1	16 mm ballscrew L=725, L1=625	\$460.00	\$460.00
2	Fixed Bearing w/slotted nut	\$245.00	\$490.00
2	Floating Bearing	\$11.80	\$23.60
2	16 mm Ball Nut	Incl w/Bscrw	
2	16 mm Ball Nut Housing	\$88.47	\$176.94
2	Housing nut for fixed bearing	Incl w/Brng	
2	Motor	\$30.00	\$60.00
2	Encoder, 800 steps/rev	\$100.00	\$200.00
2	Bellows, X	\$112.95	\$225.90
2	Bellows, Y	\$47.30	\$94.60
2	Flexible Coupling, 1/4", Encoder	\$20.00	\$40.00
2	Flexible Coupling, 5/16", Motor	\$60.00	\$120.00
4	Stainless Steel Set-Screw Collars	\$1.47	\$5.88
2	1/4 inch rod, 42.7 inches long	\$6.33	\$12.66
21	3/16 inch x 2 x 23.5 Hot Dipped Galvanized Fins	\$4.00	\$84.00
Machined Parts			
1	Stiffner, X-axis, From Flat Ground Stock	\$250.00	\$250.00
1	Dual Mountplate, From Flat Ground Stock	\$500.00	\$500.00
1	Bearing Block, X, Motor	\$815.00	\$815.00
1	Bearing Block, X, Encoder	\$710.00	\$710.00
1	Bearing Block, Y, Motor	\$260.00	\$260.00
1	Bearing Block, Y, Encoder	\$235.00	\$235.00
1	Nut Mounting Plate, X	\$230.00	\$230.00
1	Nut Mounting Plate Cover, X	\$200.00	\$200.00
1	Nut Mounting Plate, Y	\$130.00	\$130.00
1	Nut Mounting Plate Cover, Y	\$110.00	\$110.00
8	Bellows Endplates (each slightly different)	\$35.00	\$280.00
1	Tank	\$1,460.00	\$1,460.00
	Assembly cost ~10 hrs @ 20/hr	\$200.00	\$200.00
* parts quoted in quantities of 100			Estimated Ccost of Machine \$9,048.15

5.8 Conclusion

This thesis documents the design of a small and inexpensive abrasive waterjet cutter, from the specification of functional requirements, to concept generation, concept selection, prototype testing, through to final design and solid modeling of the entire machine and all of

its parts. Presented herein and shown in Figure 5.16 is the design of the finished machine. It uses an X-Y system of travel for nozzle placement and a novel structural system which is comprised of the linear guide rails.

This waterjet cutter is designed to meet a number of functional requirements set forth in the introduction to this thesis. These functional requirements include a 13 in x 26 in machinable area (modified from 26 in x 26 in), a top speed of 180 in/min, a maximum acceleration of 0.1 g's, a resolution of .0005 in/step or finer, and a cost (including arms, table, and controls) of \$10,000 or less. The first functional requirement is met with the design of the x and y axes. The functional requirements referring to speed, acceleration, and resolution were considered during the selection of ballscrews, motors, and encoders such that the the correct components were chosen to meet these specifications. Lastly, though the design of the control system is not address in this thesis, the cost of the machine, allowing around \$1,000 for controls, falls within the original cost goal of \$10,000. All this is accomplished with a design that is simple and elegant and uses a novel approach for its structure.

5.9 Future Work

A prototype of the abrasive waterjet cutter designed in this thesis should be built and tested to verify that it meets all the functional requirements. In addition, the controls need to be developed that will control this machine. Also, the motor that is specified in the design is an inexpensive motor that meets the torque and speed requirements, however it needs to be tested in conjunction with a controller to verify that it has the resolution and response required to successfully and accurately drive the axes of the machine to meet the functional requirements.

Once a prototype is built and tested, the design can be modified to reflect any improvements needed to meet any functional requirements, to reduce cost, or to increase ease of manufacture.

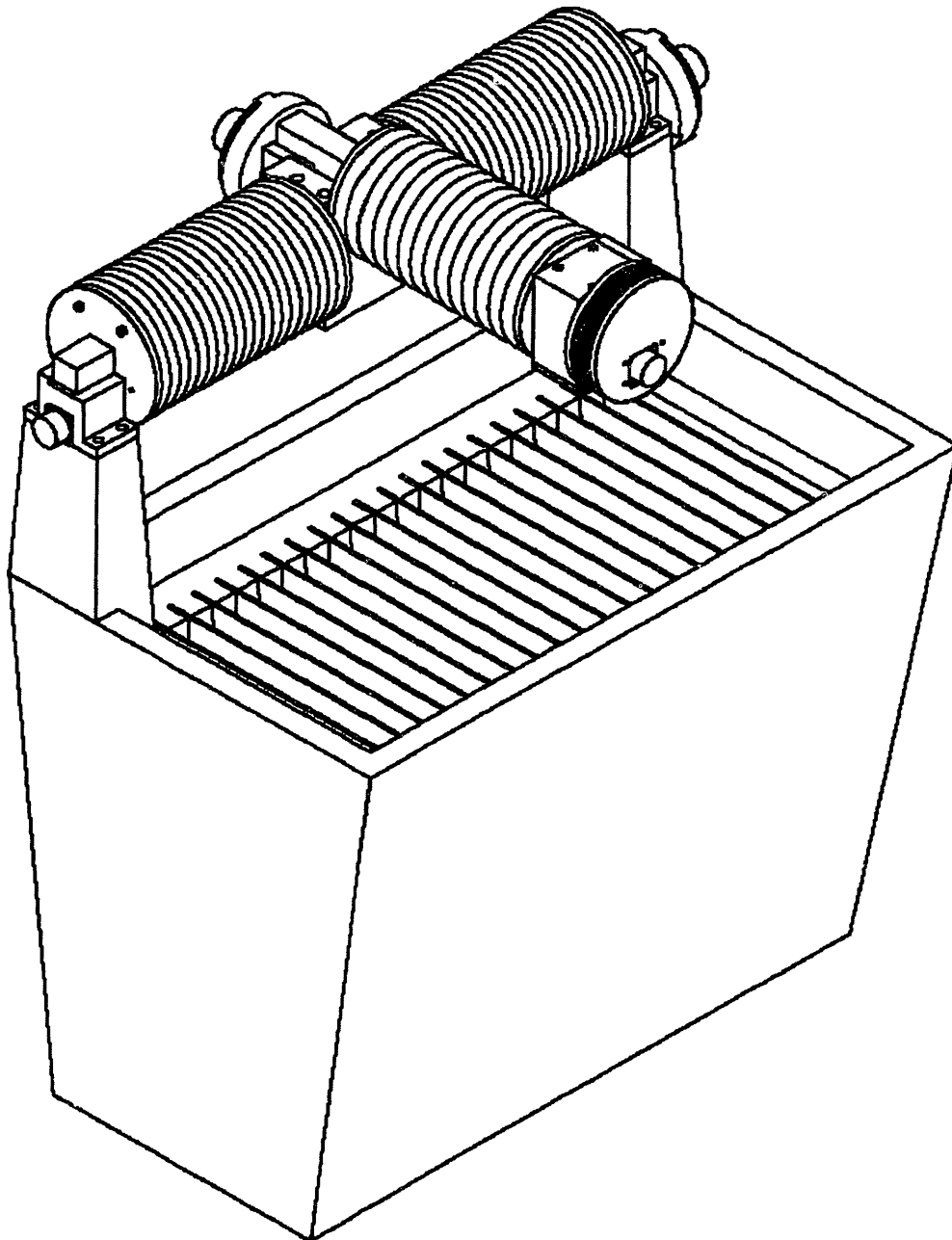


Figure 5.16 Solid Model of Finished Design

REFERENCES

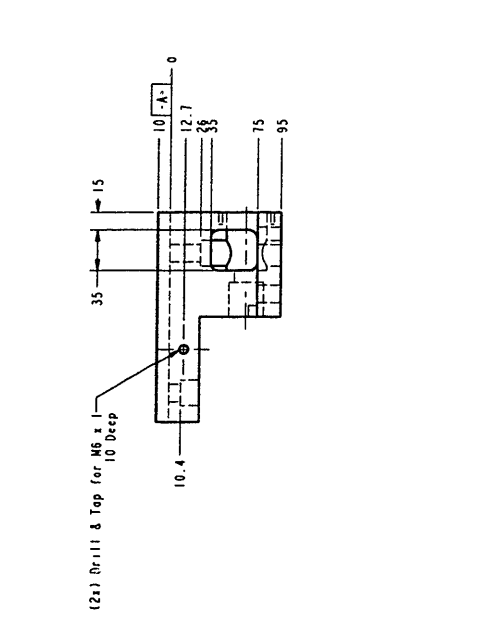
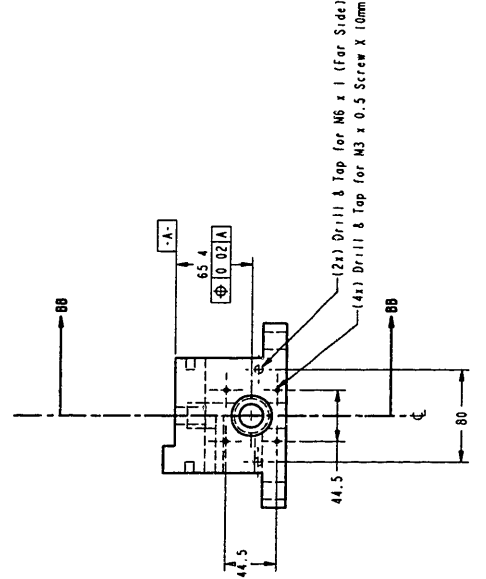
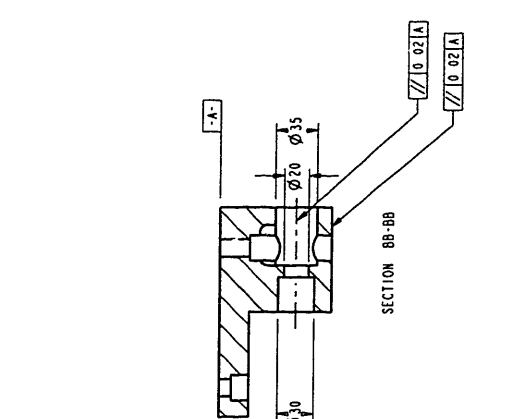
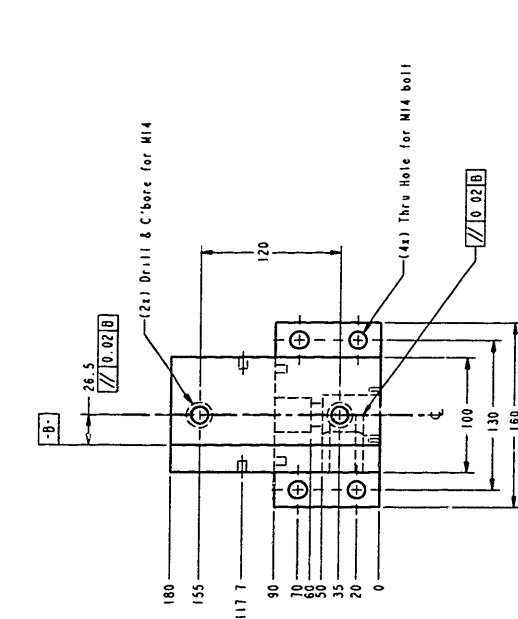
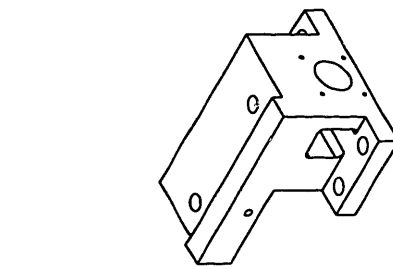
- [Slocum, 1992] Slocum, H. Alexander, *Precision Machine Design*, Prentice-Hall inc., New Jersey, 1992.
- [Meirovitch, 1986] Meirovitch, Leonard, *Elements of Vibration Analysis*, McGraw-Hill, Inc., New York, 1986
- [Green, 1996] Green, Robert E., Editor, *Machinery's Handbook, 25th Edition*, Industrial Press Inc., New York, 1996
- [Shigley and Mischke, 1989] Shigley, Joseph and Mischke, Charles, *Mechanical Engineering Design*, McGraw-Hill, Inc., New York, 1989

Appendix A

ENGINEERING DRAWINGS

ZONE	REV	REV NO	DESCRIPTION	BY	DATE	APPROVED
			NEW RELEASE			

FORM NO	1	REV	A
DATE	5	DATE	



Bearing Block, X, Encoder
Mat'l: Steel
Qty: 1

REFERENCES	DATE	BY	REV
0.0	24.15	MIT	1
0.0	24.15	MIT	2
0.000	24.15	MIT	3
0.000	24.15	MIT	4
0.000	24.15	MIT	5
0.000	24.15	MIT	6
0.000	24.15	MIT	7
0.000	24.15	MIT	8
0.000	24.15	MIT	9
0.000	24.15	MIT	10
0.000	24.15	MIT	11
0.000	24.15	MIT	12
0.000	24.15	MIT	13
0.000	24.15	MIT	14
0.000	24.15	MIT	15
0.000	24.15	MIT	16
0.000	24.15	MIT	17
0.000	24.15	MIT	18
0.000	24.15	MIT	19
0.000	24.15	MIT	20
0.000	24.15	MIT	21
0.000	24.15	MIT	22
0.000	24.15	MIT	23
0.000	24.15	MIT	24
0.000	24.15	MIT	25
0.000	24.15	MIT	26
0.000	24.15	MIT	27
0.000	24.15	MIT	28
0.000	24.15	MIT	29
0.000	24.15	MIT	30
0.000	24.15	MIT	31
0.000	24.15	MIT	32
0.000	24.15	MIT	33
0.000	24.15	MIT	34
0.000	24.15	MIT	35
0.000	24.15	MIT	36
0.000	24.15	MIT	37
0.000	24.15	MIT	38
0.000	24.15	MIT	39
0.000	24.15	MIT	40
0.000	24.15	MIT	41
0.000	24.15	MIT	42
0.000	24.15	MIT	43
0.000	24.15	MIT	44
0.000	24.15	MIT	45
0.000	24.15	MIT	46
0.000	24.15	MIT	47
0.000	24.15	MIT	48
0.000	24.15	MIT	49
0.000	24.15	MIT	50
0.000	24.15	MIT	51
0.000	24.15	MIT	52
0.000	24.15	MIT	53
0.000	24.15	MIT	54
0.000	24.15	MIT	55
0.000	24.15	MIT	56
0.000	24.15	MIT	57
0.000	24.15	MIT	58
0.000	24.15	MIT	59
0.000	24.15	MIT	60
0.000	24.15	MIT	61
0.000	24.15	MIT	62
0.000	24.15	MIT	63
0.000	24.15	MIT	64
0.000	24.15	MIT	65
0.000	24.15	MIT	66
0.000	24.15	MIT	67
0.000	24.15	MIT	68
0.000	24.15	MIT	69
0.000	24.15	MIT	70
0.000	24.15	MIT	71
0.000	24.15	MIT	72
0.000	24.15	MIT	73
0.000	24.15	MIT	74
0.000	24.15	MIT	75
0.000	24.15	MIT	76
0.000	24.15	MIT	77
0.000	24.15	MIT	78
0.000	24.15	MIT	79
0.000	24.15	MIT	80
0.000	24.15	MIT	81
0.000	24.15	MIT	82
0.000	24.15	MIT	83
0.000	24.15	MIT	84
0.000	24.15	MIT	85
0.000	24.15	MIT	86
0.000	24.15	MIT	87
0.000	24.15	MIT	88
0.000	24.15	MIT	89
0.000	24.15	MIT	90
0.000	24.15	MIT	91
0.000	24.15	MIT	92
0.000	24.15	MIT	93
0.000	24.15	MIT	94
0.000	24.15	MIT	95
0.000	24.15	MIT	96
0.000	24.15	MIT	97
0.000	24.15	MIT	98
0.000	24.15	MIT	99
0.000	24.15	MIT	100

MIT
MASSACHUSETTS INSTITUTE OF TECHNOLOGY
300 MASSACHUSETTS AVENUE
CAMBRIDGE, MASSACHUSETTS 02139
TEL: 617-253-3000
FAX: 617-253-3000
WWW: WWW.MIT.EDU

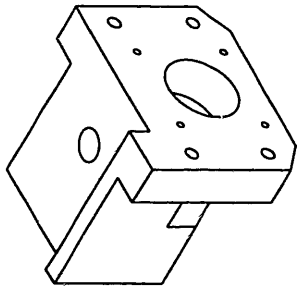
DATE: 24.15
BY: MIT
REV: A

SCALE: 1:1

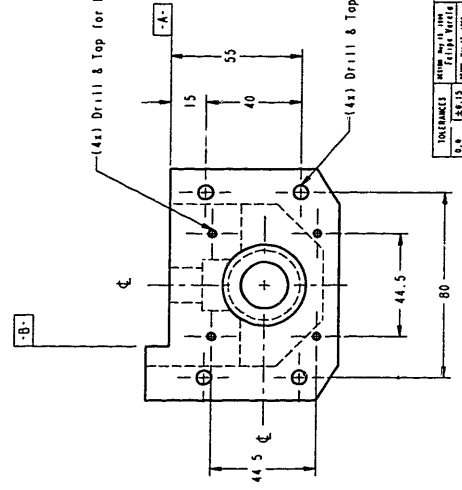
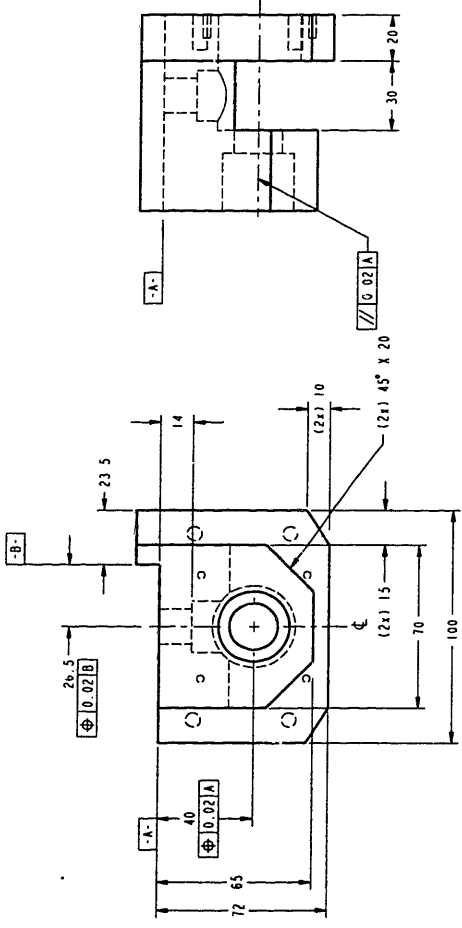
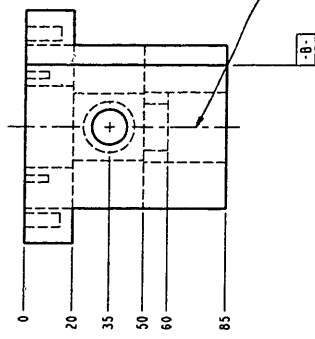
CODE IDENT: 31413

SHEET 5 OF 13

ZONE	REV	SEC NO	REV	DATE	APPROVED
DECLARATION			DATE	BY	BY
NEW RELEASE					



Bearing Block, Y, Encoder
 Mat'l: Aluminum
 Finish: Black Anodize
 Qty 1

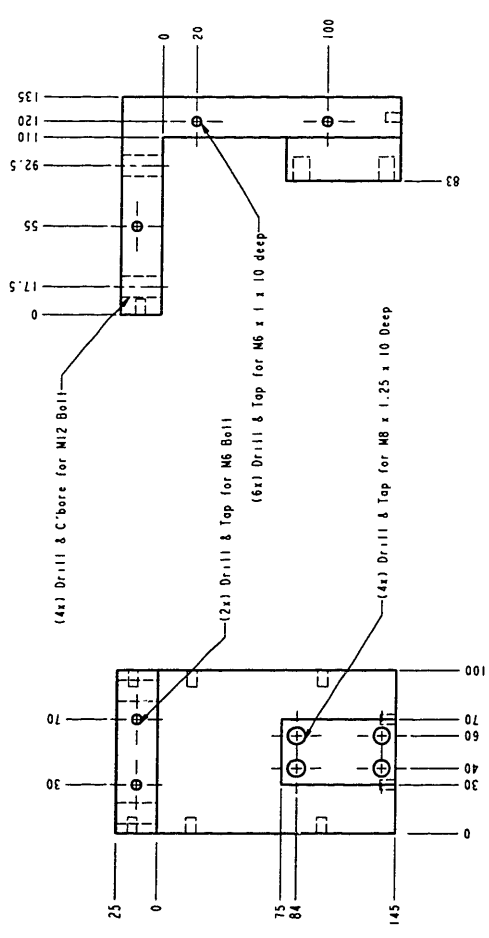


DATE	REV	BY	APP
7	A		
MIT			
Materjel			
PART NO			
DRAWING NO			
PROJ NAME FILE			
SCALE			
SHEET 1 OF 13			

TOLERANCES	UNLESS SPECIFIED
FRACTIONS	± 0.005
DECIMALS	± 0.005
ANGLES	± 0.5°
HOLE DRILLING	
SIZE	± 0.005
HOLE POSITION	
SIZE	± 0.005

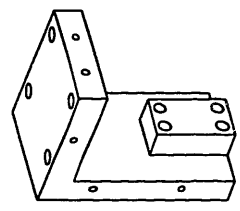
1 2 3 4 5 6 7 8

FORM NO	1	REV	A
DATE	10/15/68	BY	BT
DESCRIPTION	NET MOUNTING PLATE COVER, Y		
NEW RELEASE	APPROVED		

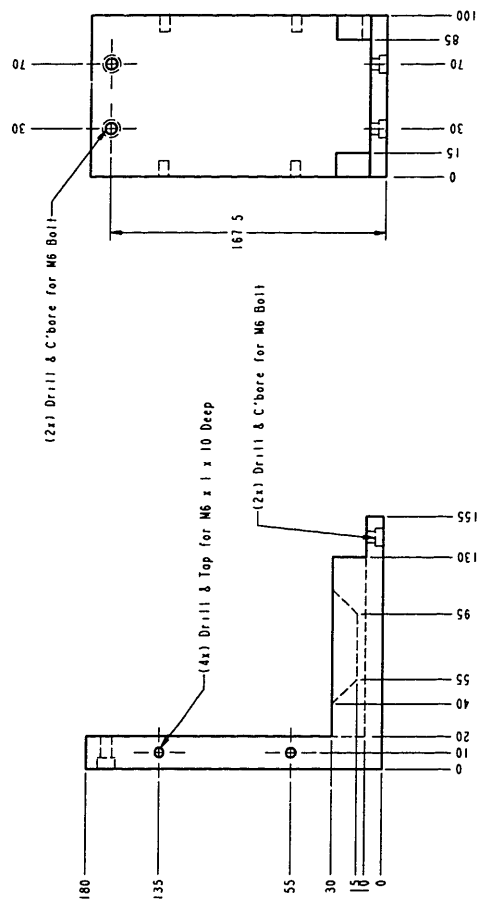


SCALE 0 500

Net Mounting Plate, Y
 Mat'l: Aluminum
 Finish: Black Anodize
 Qty: 1



Net Mounting Plate Cover, Y
 Mat'l: Aluminum
 Finish: Black Anodize
 Qty: 1



SCALE 0 500

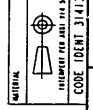
DATE	10/15/68	BY	BT
DESCRIPTION	NET MOUNTING PLATE COVER, Y		
NEW RELEASE	APPROVED		

FORM NO	1	REV	A
DATE	10/15/68	BY	BT
DESCRIPTION	NET MOUNTING PLATE COVER, Y		
NEW RELEASE	APPROVED		

FORM NO	1	REV	A
DATE	10/15/68	BY	BT
DESCRIPTION	NET MOUNTING PLATE COVER, Y		
NEW RELEASE	APPROVED		

FORM NO	1	REV	A
DATE	10/15/68	BY	BT
DESCRIPTION	NET MOUNTING PLATE COVER, Y		
NEW RELEASE	APPROVED		

FORM NO	1	REV	A
DATE	10/15/68	BY	BT
DESCRIPTION	NET MOUNTING PLATE COVER, Y		
NEW RELEASE	APPROVED		



MIT
 MATERIALS
 MIT
 MIT

SCALE 0 500

NET MOUNTING PLATE COVER, Y

MIT

MIT

MIT

MIT

MIT

MIT

MIT

MIT

MIT

MIT

MIT

MIT

MIT

MIT

MIT

MIT

MIT

THESIS PROCESSING SLIP

FIXED FIELD: ill. _____ name _____

index _____ biblio _____

► COPIES: Archives Aero Dewey Eng Hum
Lindgren Music Rotch Science

TITLE VARIES: ► _____

NAME VARIES: ► Felipe Alonso

IMPRINT: (COPYRIGHT) _____

► COLLATION: III P

► ADD: DEGREE: _____ ► DEPT.: _____

SUPERVISORS: _____

NOTES:

cat'r:

date:

page:

► DEPT: H.E. ► 3142

► YEAR: 1999 ► DEGREE: S.M.

► NAME: VARELA, Felipe